

**Improving Proppant Placement Efficiency Using the Self-generated Gas Floating
Technique**

by

Yikun Li

A thesis submitted in partial fulfillment of the requirements for the degree of

Master of Science

in

Petroleum Engineering

Department of Civil and Environmental Engineering
University of Alberta

© Yikun Li, 2024

ABSTRACT

Hydraulic fracturing plays an essential role in producing unconventional hydrocarbon resources. The success of hydraulic fracturing operations and the performance of developing unconventional hydrocarbon resources strongly depend on the distribution of proppants in the induced fractures. Proppants establish effective flowing paths with high conductivity for reservoir fluids by preventing the closure of the induced fractures. However, due to the gravitational force, proppants tend to settle down rapidly in the induced vertical fractures. This behaviour leads to the closure of the unproped fracture at the higher sections after the hydraulic fracturing operation and a lower filling efficiency. Many studies on proppants have been made to improve the proppant filling efficiency. However, they are limited to the methods mainly focused on reducing proppants' density or increasing the buoyancy force of fracturing fluid. One particular study suggests utilizing gas-suspended proppants to increase the proppant placement efficiency at the higher sections of fractures (Wang *et al.*, 2017). The authors recommend injecting nitrogen along with proppants and fracturing fluid during the slurry stage of hydraulic fracturing operations. The nitrogen gas bubbles attach and bring proppants to the higher section of the fracture. To minimize the cost of nitrogen and the complexity of hydraulic fracturing operations, we desire to examine if gas bubbles can be generated inside fractures to improve proppant placement efficiency. Here, the self-generated gas floating technique is proposed in this study for the first time. This technique adds an external lifting force to proppants from the reaction-generated CO₂ bubbles. It incorporates the proppants' surface characteristics to bring the proppants to a higher fracture location and increases the proppant filling efficiency.

In this study, we first alter the wettability of ceramic proppants using a siliconizing chemical called SurfaSil and measure the contact angles of three type of proppants (i.e., ceramic proppants, resin-coated proppants and SurfaSil-treated proppants). Then, we evaluate the adhesion forces between resin-coated proppants and CO₂/air. Furthermore, we apply the self-generated gas floating technique in a transparent fracture model to study the proppant placement efficiency at the laboratory condition. We study the effects of proppant size, proppant wettability, reaction rate, fracture width and gas bubble types on the proppant placement efficiency (i.e., the ratio of the area occupied by proppants to the total fracture area). The proppant placement efficiency is quantified through the MATLAB image analysis codes. In conclusion, there is a proportional relationship between the reaction rate and proppant placement efficiency. A larger fracture width also tends to increase the proppant placement efficiency. There is an inverse relationship between the size of proppants and the proppant placement efficiency. Among the different proppant types, resin-coated proppants are proven to yield the highest proppant placement efficiency in the fracture model.

Next, we analyze the actual wellhead pressure recorded by one field hydraulic fracturing operation and find that the pressure decline rate is about 40 MPa/min after the pumping of proppant slurry. We then adopt pressure decline rates similar to the field decline rate of 40 MPa/min in high-pressure experiments to examine whether the self-generated gas floating technique can actually work. In our high-pressure experiments, we first pressurize the reactor that is filled with resin-coated proppants and sodium bicarbonate solution to 10 MPa using CO₂. Subsequently we inject acetic acid into the reactor. Lastly, we decrease the pressure in the reactor under different rates to simulate the pressure decline stage after

the hydraulic fracturing operation. During the experiments, we initiate the acid and base reactions under two different pressure decline rates and visually evaluate whether the self-generated CO₂ bubbles can lift the resin-coated proppants that are originally located at the bottom of the reactor. From the high-pressure experiments, we can conclude that the chemical reaction cannot be initiated if we maintain high-pressure conditions. If we decline the pressure at a high rate, the reaction rate becomes faster to generate a larger amount of CO₂ bubbles that push proppants upward. If the pressure decline rate is low, the reaction rate is low, and only a few CO₂ bubbles are generated, which can barely attach and bring the proppants to the higher location in the reactor.

Dedication

This thesis is dedicated to my mother, Lijie Yang and my father, Guohua Li.

Acknowledgments

I am grateful to everyone who guided and supported me in the past six years of study at the University of Alberta. First, I would like to express my sincere gratitude to my mother, Lijie Yang, and my father, Guohua Li, who have always financially and mentally supported me. I could have not reached this stage without their help.

I also sincerely thank my supervisors, Dr. Huazhou (Andy) Li and Dr. Tayfun Babadagli. I appreciate their valuable knowledge, patience, and guidance throughout my Master of Science program. I am incredibly fortunate to be supervised by them.

I acknowledge the essential help from Georgeta Istratescu and John F. Czuroski, who provided countless technical support for my experiments. Their support makes my experiments possible.

In addition, I appreciate PETRONAS Canada for providing the measured wellhead pressure profiles during a hydraulic fracturing operation.

Table of Contents

ABSTRACT.....	ii
Dedication.....	v
Acknowledgments.....	vi
List of Tables	x
List of Figures	xi
Chapter 1: Introduction.....	1
1.1 Background.....	1
1.2 Literature Review.....	3
1.3 Problem Statement.....	7
1.4 Research Objectives.....	8
1.5 Thesis Structure	9
References.....	10
Chapter 2: Proppant Wettability Measurements and the Application of the Self-generated Gas Floating Technique under Ambient Conditions	14
2.1 Introduction.....	14
2.2 Experimental Section.....	17
2.2.1 Materials	17
2.2.2 Experimental setup.....	18
2.2.3 Experimental procedures	27

2.3 Results and Discussion	32
2.3.1 Contact angle of a water droplet on proppants	32
2.3.2 Contact angle of an air/CO ₂ bubble on proppants	34
2.3.3 Adsorption of air/CO ₂ bubbles on proppants.....	37
2.3.4 Results of the self-generated gas floating experiments.....	38
2.4 Conclusions.....	47
References.....	48
Chapter 3: A Visual Experimental Study: The Application of the Self-generated Gas Floating Technique under Reservoir Conditions	
	50
3.1 Introduction.....	50
3.2 Experimental Section	54
3.2.1 Materials	54
3.2.2 Experimental setup.....	55
3.2.3 Experimental procedure	57
3.3 Results and Discussion	58
3.3.1 Pressurization of the reactor using CO ₂	58
3.3.2 Acid injection process.....	62
3.3.3 Effect of pressure decline rates	65
3.4 Conclusions.....	76
References.....	77
Chapter 4: Conclusions and Recommendations	78

4.1 Conclusions.....	78
4.2 Recommendations.....	80
Bibliography	81
Appendix: Complete Image Analysis Results from the Self-generated Gas Floating Experiments in Chapter 2.....	87

List of Tables

Table 2.1 Properties of ceramic proppants and resin-coated proppants with different mesh sizes.....	18
Table 2.2 Experimental variables and the corresponding values used in the self-generated gas floating experiments	23
Table 2.3 Experimental schedules used in the self-generated gas floating experiments .	23
Table 3.1 Properties of resin-coated proppants with mesh size 30/50	54
Table 3.2 Experimental parameters of the high-pressure experiments	56
Table A.1 Complete results of the self-generated gas floating experiment in Chapter 2	108

List of Figures

Figure 1.1 Summary of different approaches developed in the past to increase the proppant placement efficiency in fractures	7
Figure 2.1 Schematic of SurfaSil coating experiment	19
Figure 2.2 Schematic of experimental setup used to measure the contact angle of a water droplet on ceramic proppants, resin-coated proppants and SurfaSil-treated proppants....	20
Figure 2.3 Schematic of the experimental setup used to measure the contact angle of an air or CO ₂ bubble on resin-coated proppants in an aqueous condition	21
Figure 2.4 Schematic of the experiment setup used to reveal the adsorption of air/CO ₂ bubbles onto proppants	21
Figure 2.5 Schematic of the self-generated gas floating experiments	22
Figure 2.6 Distribution of resin-coated proppants with a mesh size of 30/50 in the investigated zone in the 4 mm wide fracture model. The image is captured prior to the injection of acid to the fracturing fluid with 8 wt% of sodium bicarbonate. The left image is the original image, while the right one is the processed image. The proppant coverage ratio is measured to be 0.	32
Figure 2.7 Distribution of resin-coated proppants with a mesh size of 30/50 in the investigated zone in the 4 mm wide fracture. The image is captured post the injection of acid with the rate of 21 ml/min to the fracturing fluid with 8 wt% of sodium bicarbonate. The left image is the original image, while the right one is the processed image. The proppant coverage ratio is measured to be 0.28262.....	32
Figure 2.8 Contact angle of one water droplet on ceramic proppants with a mesh size of 30/50	33

Figure 2.9 Contact angle of one water droplet on resin-coated proppants with a mesh size of 30/50 33

Figure 2.10 Contact angle of one water droplet on SurfaSil-treated proppants with a mesh size of 30/50 34

Figure 2.11 Contact angle of an air bubble on ceramic proppants in water 35

Figure 2.12 Contact angle of a CO₂ bubble on ceramic proppants in water 35

Figure 2.13 Contact angle of an air bubble on resin-coated proppants in water 36

Figure 2.14 Contact angle of a CO₂ bubble on resin-coated proppants in water 36

Figure 2.15 Contact angle of an air bubble on SurfaSil-treated proppants in water 37

Figure 2.16 Contact angle of a CO₂ bubble on SurfaSil-treated proppants in water 37

Figure 2.17 Comparison of the interaction between air/CO₂ and different proppants: (a) Resin-coated proppants with air; (b) Resin-coated proppants with CO₂; (c) Ceramic proppants with CO₂ 38

Figure 2.18 Coverage ratio of each type of proppant after air injection at a rate of 21 ml/min in the fracture model with a width of 4 mm (left) and in the fracture model with a width of 1.5 mm (right) 40

Figure 2.19 Coverage ratio of each type of proppant after the acid injection at a rate of 21 ml/min into the 4 wt% sodium bicarbonate fracturing fluid in the fracture model with a width of 4 mm (left) and in the fracture model with a width of 1.5 mm (right) 40

Figure 2.20 Coverage ratio of each type of proppant after the acid injection at a rate of 10 ml/min into the 4 wt% sodium bicarbonate fracturing fluid in the fracture model with a width of 4 mm (left) and in the fracture model with a width of 1.5 mm (right) 40

Figure 2.21 Coverage ratio of each type of proppant after the acid injection at a rate of 10 ml/min into the 8 wt% sodium bicarbonate fracturing fluid in the fracture model with a width of 4 mm (left) and in the fracture model with a width of 1.5 mm (right)..... 41

Figure 2.22 Coverage ratio of each type of proppant after the acid injection at a rate of 21 ml/min into the 8 wt% sodium bicarbonate fracturing fluid in the fracture model with a width of 4 mm (left) and in the fracture model with a width of 1.5 mm (right)..... 41

Figure 2.23 Coverage ratio of each type of proppant after the acid injection at a rate of 21 ml/min into the 4 wt% sodium bicarbonate fracturing fluid in the fracture model with a width of 1.5 mm..... 42

Figure 2.24 Interaction of resin-coated proppants with reaction-generated CO₂ 44

Figure 2.25 Coverage ratio of each type of proppant after air injection at a rate of 21 ml/min in the fracture model with a width of 4 mm (left) and coverage ratio of each type of proppant after the acid injection at a rate of 10 ml/min into the 4 wt% of sodium bicarbonate fracturing fluid in the fracture model with a width of 4 mm (right)..... 45

Figure 2.26 Coverage ratio of each type of proppant with the mesh size of 30/50 after the acid injection at a rate of 21 ml/min into the 8 wt% sodium bicarbonate fracturing fluid in the fracture model with a width of 4 mm versus the contact angle of a CO₂ bubble on each type of proppant 46

Figure 3.1 Hydraulic-fracturing field data provided by PETRONAS Canada 51

Figure 3.2 Retrieved pressure data from a hydraulic fracturing operation done by PETRONAS Canada..... 51

Figure 3.3 Schematic showing the experimental setup used to conduct the self-generated gas floating experiment under high-pressure conditions 56

Figure 3.4 Images captured during the process of pressurizing the reactor.....	61
Figure 3.5 Images captured during the process of acid injection into the reactor	64
Figure 3.6 Proppant distribution states in the reactor at different times at a pressure decline rate of 0.69 MPa/min	70
Figure 3.7 Proppant distribution states in the reactor at different times at a pressure decline rate of 5 MPa/min	74

Chapter 1: Introduction

1.1 Background

As worldwide energy consumption keeps increasing, the further improvement and optimization of well stimulation methods (such as hydraulic fracturing) become more urgent. Hydraulic fracturing technology was first developed and implemented in 1949 to increase gas production in Oklahoma (Montgomery and Smith, 2010). Hydraulic fracturing aims to induce fractures along the wellbore by injecting high-pressure fracturing fluid. Later, in the 1980s, operators started to perform hydraulic fracturing operations in horizontal wells when developing hydrocarbon resources from tight reservoirs (Zhang *et al.*, 2021). The horizontal-well hydraulic fracturing operation induces multi-stage fractures along the horizontal section of the well. The induced fractures along the horizontal well generate a much larger drainage area than the single-stage fractures induced in a vertical well.

The hydraulic fracturing operation typically consists of three stages: the pad stage, the slurry stage, and the completion stage. Fractures are induced by injecting high-pressure and solid-free fracturing fluid through perforations during the pad stage. Then, a mixture of fracturing fluid and proppants is injected into the fractures induced by the pad fluids. Upon the completion of the fracturing operation, a soaking period normally ensues. Then, the pressure inside the fractures decreases dramatically, and the fractures will be closed to some extent due to the in-situ stresses (Wang *et al.*, 2014). After soaking, part of the fracturing fluid flows back from the fractures to the surface (Guo *et al.*, 2007; Sarmadivaleh, 2012). Proppants remain in the fractures to maintain the openings of the fractures. As such,

the fractures with a high fracture conductivity can be established and they are more accessible for the trapped hydrocarbon to flow into the wellbore. Herein, fracture conductivity is used to describe how easily the reservoir fluids flow to the wellbore through the fractures (Ma *et al.*, 2016). A wider fracture usually provides a higher reservoir conductivity and vice versa. Proppants are critical in hydraulic fracturing because they keep the induced hydraulic fractures open and ensure the connectivity between the reservoir and the wellbore. The proppants inside the fractures should be strong enough to resist the high in-situ stresses and keep the fractures open. In order to adapt to a variety of reservoir conditions, the proppants can be coated with a layer of epoxy resin to make them more chemically and thermally resistant (Wei, 2019). The resin coating can mitigate the proppant-debris flowback problem (Fan *et al.*, 2021). In addition, the particle size of the proppants is another important influential factor affecting the performance of supporting the induced fractures. To support the induced fractures effectively, the mesh size of the proppants used in hydraulic fracturing operations usually ranges from mesh size 8 to mesh size 140 (Liang *et al.*, 2016). Proppants with a smaller mesh size are larger in actual size. The proppants with a smaller mesh size are easier to be crushed than those with a larger mesh size when they are subjected to the in-situ stresses. However, using the proppants with a smaller mesh size in hydraulic fracturing can help yield a larger fracture conductivity (Guo *et al.*, 2017).

Proppant filling is one of the most critical problems directly influencing the hydrocarbon production performance of a given fractured well. Before the closure of fractures, proppants tend to fall inside fractures due to the gravitational force. This phenomenon is

unfavourable since the upper part of fractures is sometimes left unpropped, which leads to a poor fracture conductivity (Britt *et al.*, 2006).

1.2 Literature Review

Silica sand and ceramic proppant are the two most widely used proppants in hydraulic fracturing operations because they are low-cost (Liang *et al.*, 2016). Silica sand is environmentally friendly and easily found in nature. However, silica sand grains are easily crushed when they are applied to high in-situ stresses in the induced fractures. The crushed sand grains tend to flow back to the wellbore, leading to damage to the downhole equipment and the reduction of fracture conductivity (Liu *et al.*, 2023). Therefore, silica sand is only applicable in low-in-situ stress formations. Unlike silica sand, ceramic proppants are more spherical and can withstand a much higher compressive stress (Liang *et al.*, 2016). Proppant manufacturers increase the sphericity and roundness of proppants to improve their stress-bearing capacity. The packing of spherical proppants yields a larger porous space in the proppants bed than using the proppants with non-spherical shapes (Liang *et al.*, 2020). Resin-coated proppant is more advantageous than ceramic proppant, though it is more expensive. An additional layer of resin is coated on the surface of the proppant to make it more chemically and thermally resistant (Wei, 2019). In addition, if a resin-coated proppant is crushed in the fracture, the resin layer can restrict the motion of proppant debris by confining the debris within the resin coating. Moreover, resin-coated proppants can form proppant aggregates when being immersed in a fracturing fluid. This can mitigate the proppant flowback problem during the completion and hydrocarbon production stages.

Several studies have investigated how to maximize the proppant placement efficiency in vertical fractures by modifying the viscosity of fracturing fluid and optimizing the density of proppants (Liang *et al.*, 2016; Belyadi *et al.*, 2019). One commonly used method is adding linear gels to the fracturing fluids to increase their viscosity. For example, guar is one of the most widely used linear gels in hydraulic fracturing operations because it is cheap. Increasing the viscosity of fracturing fluid decreases the settling velocity of proppants in the fracturing fluid. A more viscous fracturing fluid creates more extensive fractures. It reduces the effect of reservoir tortuosity and achieves a better filling of proppants in fractures (Horwitt, 2017). In addition, the use of highly viscous fracturing fluid prevents the fluid from leaking into the rock matrix, but may cause formation damage (Li *et al.*, 2022). Another drawback of using the viscous fracturing fluid is the slower injection rate since the frictional pressure drop in the tubing is larger.

Many proppant technologies are invented to maximize the proppant placement efficiency by reducing the density of the used proppants. For example, the self-suspending proppant is one of the technologies to decrease the density of the proppants. The self-suspending proppant is prepared by coating a layer of hydrogel on the proppant to achieve a longer suspension time in the fracturing fluid (Mahoney *et al.*, 2013). Increasing the thickness of hydrogel immersed in fracturing fluid decreases the bulk density of the proppant so that the self-suspending proppant can achieve a longer suspension time in the fracturing fluid. Another method of preparing the self-suspending is modifying the surface coating of the proppants. The coating can be dissolved in the fracturing fluid to increase the viscosity of the surrounding fracturing fluid. As such, the settling velocity of the proppants in the

fracturing fluid can be significantly decreased (Danso *et al.*, 2021). Another proppant technology is called the ultra-low weight proppant. Ultra-low weight proppants are developed either by increasing the porosity of the proppants or by using ultra-low weight materials when manufacturing the proppants (Feng *et al.*, 2021). The proppants are porous and hollow, so they have a lighter weight. The materials used to make the ultra-low weight proppants are composite and polymerized, which can have a much lower density than sands and ceramics. When the ultra-low weight proppants are immersed in the fracturing fluid, the relative density between the ultra-low weight proppants and the fracturing fluid is low, resulting in a low settling velocity of the proppants. Thus, a more uniform proppant placement in the upper part of the induced fractures can be achieved by using ultra-low weight proppants. However, the ultra-low weight proppants are difficult to be widely used because of their poor performance in resisting the high in-situ stresses. An alternative proppant technology is called the gas-suspended proppant, which utilizes the gas bubbles to provide an upward lifting force on proppants to increase the proppant placement efficiency at the upper section of the induced fractures. One study touched on how to prepare the gas-suspended proppants (Wang *et al.*, 2017). The first step is to coat a layer of hydrophobic and gas-wet material on the ceramic proppants. Subsequently, nitrogen is mixed with the treated ceramic proppants in slick water to prepare the fracturing fluid. The volume of nitrogen is around 10-20% of the total volume of the fracturing fluid. Then, we inject the mixed fracturing fluid into the formation. Nitrogen gas will provide an upward force when they are attracted by the treated hydrophobic ceramic proppants to extend the suspension time in the fracturing fluid. However, this process is complex and expensive.

Based on the literature review, we summarize the approaches developed in the past to extend the suspension time of proppants in a fracturing fluid, as shown in Figure 1.1. Using these methods, we may achieve a higher proppant placement efficiency by reducing the relative density between proppants and fracturing fluids. However, these methods are costly and with high complexity. To reduce the complexity and cost, we propose a new method called the self-generated gas floating technique to generate in-situ gas bubbles inside the hydraulically induced fractures. As such, the proppant placement efficiency can be improved because the generated in-situ gas bubbles can attach and bring the proppants to a higher location in the induced fractures. The CO₂ gas bubbles are produced through the acid-base reaction, as shown in Equation 1.1. We first add sodium bicarbonate to the fracturing fluid to make the fracturing fluid alkaline. Then, we start injecting the alkaline fracturing fluid into the induced fracture. We subsequently prepare and inject acidic fracturing fluid by mixing acetic acid with the fracturing fluid. The chemical reaction takes place inside the induced fractures, and the generated CO₂ bubbles can bring the proppants to the higher section of the fractures.





Figure 1.1 Summary of different approaches developed in the past to increase the proppant placement efficiency in fractures

1.3 Problem Statement

It is important to consider the cost-effectiveness and the complexity of the hydraulic fracturing process when implementing a new proppant technology. The increase in the viscosity of the fracturing fluid may cause formation damage. Also, a more powerful pump is required to inject the fracturing fluid into the wellbore because of the high frictional pressure drop. Most proppant technologies aforementioned in the literature review are costly. The compressive strengths of the ultra-low weight proppants are low due to their hollow structure. The operational procedure of the gas-suspended proppants is complex. Meanwhile, using the gas-suspended proppants requires additional nitrogen pumping units on the surface. In addition, the three-phase (solid-liquid-gas) flow in tubings increases the complexity of hydraulic fracturing operations. Hence, we propose the self-generated gas floating technique to increase the proppant placement efficiency and mitigate the drawbacks of the aforementioned proppant technologies. In our opinion, the complexity of hydraulic fracturing operations can be minimized by applying the self-generated gas

floating technique because this technique generates the in-situ CO₂ bubbles inside the induced fractures. Moreover, applying this technique doesn't require complex surface equipment such as the nitrogen pumping unit. In addition, the complexity of the flow regime is also reduced since there is only a two-phase (solid-liquid) flow in the tubing. However, to the best of our knowledge, there are no experiments that have been carried out to investigate the feasibility of the self-generated gas floating technique. Hence, this work aims to study the feasibility of the self-generated gas floating technique through experimental investigations.

1.4 Research Objectives

We propose the self-generated gas floating technique to utilize the hydrophobic proppant surface to attract reaction-generated gas bubbles, and use the gas bubbles to bring the proppants to the upper part of fractures. In this study, we aim to screen the suitable proppants for the self-generated gas floating technique and examine the feasibility of this technique under realistic conditions. The following objectives are required to be completed:

1. To prepare various proppants with different surface hydrophobicity and measure their contact angles.
2. To investigate the adhesion force between CO₂ and the surface of each type of proppants by visually examining the number of gas bubbles attached to proppants, and comparing the coverage ratios of each type of proppants in the fracture model.
3. To investigate the effects of fracture width, reaction rate, proppants hydrophobicity, and type of gas bubbles on the proppant placement efficiency of the self-generated gas floating technique at ambient conditions.

4. To study the feasibility of the self-generated gas floating technique at high pressure/temperature conditions. In particular, the effect of pressure decline rate will be investigated.

1.5 Thesis Structure

This thesis consists of four chapters described as follows:

Chapter 1. This chapter provides a general background of the hydraulic fracturing technology, the existing efforts made to achieve a higher proppant placement efficiency in fractures, and the objectives of this research.

Chapter 2. This chapter covers the proppant wettability alteration and the contact angle measurements of each type of proppants. The measurements of the adhesion force between CO₂ and different types of proppants are also included. Then, we apply the self-generated gas floating technique in a fracture model to investigate the effects of fracture width, reaction rate, proppant wettability, proppant size and types of gas bubble on the proppant placement efficiency.

Chapter 3. This chapter simulates the application of the self-generated gas floating technique during the pressure decline stage in the hydraulic fracturing process. The interaction of CO₂ bubbles and resin-coated proppants is analyzed under high pressure/temperature conditions.

Chapter 4. This chapter summarizes the critical findings of this research and provides the recommendations for future research.

References

- Barati, R., Liang, J. T. 2014. A review of fracturing fluid systems used for hydraulic fracturing of oil and gas wells. *Journal of Applied Polymer Science*, 131(16): 40375.
- Belyadi, H., Fathi, E., Belyadi, F. 2019. Hydraulic Fracturing in Unconventional Reservoirs. *Gulf Professional Publishing*.
- Britt, L. K., Smith, M. B., Haddad, Z., Lawrence, P., Chipperfield, S., Hellman, T. 2006. Water-fracs: we do need proppant after all. Paper SPE 102227 presented at the SPE Annual Technical Conference and Exhibition, San Antonio, Texas, USA.
- Cao, W., Xie, K., Lu, X., Chen, Q., Tian, Z., Lin, W. 2020. Self-suspending proppant manufacturing method and its property evaluation. *Journal of Petroleum Science and Engineering*, 192: 107251.
- Danso, D. K., Negash, B. M., Ahmed, T. Y., Yekeen, N., Ganat, T. A. O. 2021. Recent advances in multifunctional proppant technology and increased well output with micro and nano proppants. *Journal of Petroleum Science and Engineering*, 196: 108026.
- Fan, F., Li, F., Tian, S., Sheng, M., Khan, W., Shi, A., Zhou, Y., Xu, Q. 2021. Hydrophobic epoxy resin coated proppants with ultra-high self-suspension ability and enhanced liquid conductivity. *Petroleum Science*, 18(6): 1753-1759.
- Feng, Y. C., Ma, C. Y., Deng, J. G., Li, X. R., Chu, M. M., Hui, C., Luo, Y. Y. 2021. A comprehensive review of ultralow-weight proppant technology. *Petroleum Science*, 18: 807-826.
- Guo, B., Liu, X., Tan, X. 2017. Petroleum Production Engineering (Second Edition). *Gulf Professional Publishing*.

- Guo, B., Lyons, W. C., Ghalambor, A. 2007. Petroleum Production Engineering. *Gulf Professional Publishing*.
- Guo, J., Guo, H., Zhang, T., Zeng, X., Li, M., Tang, T. 2022. Experiment on proppant transport in near-well area of hydraulic fractures based on piv/ptv. *Powder Technology*, 410: 117833.
- Guo, S., Wang, B., Li, Y., Hao, H., Zhang, M., Liang, T. 2022. Impacts of proppant flowback on fracture conductivity in different fracturing fluids and flowback conditions. *ACS Omega*, 7(8): 6682-6690.
- Horwitt, D. 2017. Chapter four - hydraulic fracturing chemical disclosure: can the public know what's going into oil and natural gas wells? *Advances in Chemical Pollution, Environmental Management and Protection*, 1: 63-111.
- Li, Y., Zhou, F., Li, B., Cheng, T., Zhang, M., Wang, Q., Yao E., Liang, T. 2022. Optimization of fracturing fluid and retarded acid for stimulating tight naturally fractured bedrock reservoirs. *ACS Omega*, 7(29): 25122-25131.
- Liang, F., Sayed, M., Al-Muntasheri, G. A., Chang, F. F., Li, L. 2016. A comprehensive review on proppant technologies. *Petroleum*, 2(1): 26-39.
- Liang, X., Zhou, F., Liang, T., Huang, Y., Wei, D., Ma, S. 2020. The effect of combined proppants upon the fracture conductivity in tight gas reservoirs. *Energy Reports*, 6: 879-884.
- Liu, P., Huang, Q., Li, J., Du, J., Lu, X., Liu, J., Liu, C., Lan, X. 2023. Review and perspectives of coated proppant technology. *Energy Fuels*, 37(5): 3355-3370.
- Ma, Y. Z., Holditch, S. A. 2016. Unconventional oil and gas resources handbook. *Gulf Professional Publishing*.

- Mack, M. G., Coker, C. E. 2013. Proppant selection for shale reservoirs: optimizing conductivity, proppant transport and cost. Paper SPE 167221 presented at the SPE Unconventional Resources Conference Canada, Calgary, Alberta, Canada.
- Mahoney, R. P., Soane, D. S., Herring, M. K., Kincaid, K. P., Portilla, R. C., Wuthrich, P. 2016. Self-suspending proppants for hydraulic fracturing comprising a coating of hydrogel-forming polymer, USA Patent US9297244B2.
- Montgomery, C. T., Smith, M. B. 2010. Hydraulic fracturing: history of an enduring technology. *Journal of Petroleum Technology*, 62(12): 26-40.
- Rickards, A. R., Brannon, H. D., Wood, W. D., Stephenson, C. J. 2006. High strength, ultralightweight proppant lends new dimensions to hydraulic fracturing applications. *SPE Production & Operations*, 21(02): 212-221.
- Sarmadivaleh, M. 2012. Experimental and numerical study of interaction of a pre-existing natural interface and an induced hydraulic fracture. Doctoral thesis, Curtin University.
- Wang, L., Li, X., Ding, L., Li, N., Li, X., Liu, X., Zu, K., Meng, L. 2017. The preparation and operational instruction of a gas-suspended proppant for hydraulic fracturing using slick water, China Patent CN106832145A.
- Wang, Q., Chen, X., Jha, A. N., Rogers, H. 2014. Natural gas from shale formation – the evolution, evidences and challenges of shale gas revolution in United States. *Renewable and Sustainable Energy Reviews*, 30: 1-28.
- Wei, G. 2019. Transport Behavior of Resin-Coated Ceramic Proppants in Rough Vertical Fractures. Master thesis, University of Alberta.

- Zhang, D., Liu, Y., Luo, H., Cao, S., Cao, J., Li, X. 2021. Staged fracturing of horizontal wells in continental tight sandstone oil reservoirs: a case study of yanchang formation in western ordo basin, China. *Frontiers in Earth Science*, 9: 760976.
- Zhang, J., Liu, K., Cao, M. 2017. Experimental study on modified polyacrylamide coated self-suspending proppant. *Fuel*, 199: 185-190.
- Zhang, Y., Yan, C., Chen, T., Wang, Y. 2016. Ultra-lightweight composite proppants prepared via suspension polymerization. *Journal of Composite Materials*, 50(20): 2823-2831.

Chapter 2: Proppant Wettability Measurements and the Application of the Self-generated Gas Floating Technique under Ambient Conditions

2.1 Introduction

Hydraulic fracturing is one of the standard techniques used widely in industry to develop unconventional hydrocarbon resources such as shale oil and gas. Hydraulic fracturing operations can be implemented in both vertical and horizontal wells. The horizontal-well hydraulic fracturing operations become more popular in the 21st century. Horizontal-well hydraulic fracturing operations are done by inducing multi-stage fractures around horizontal wells using high-pressure fracturing fluid and proppants. Proppant is a critical component in hydraulic fracturing operations, and it is used to prevent the closure of hydraulically induced fractures due to in-situ stresses to maintain fracture conductivity. One long-lasting problem in hydraulic fracturing operations is the problem of poor proppant placement inside the upper part of fractures (Wang and Elsworth, 2018). Proppants tend to settle down inside fractures because of the gravitational force, and this results in the problem of insufficient proppant filling in the upper part of fractures that leads to the reduction of fracture conductivity.

Many new proppant technologies have been developed to mitigate the proppant filling problem, such as using ultra-low weight proppants and gas-suspended proppants. These proppants achieve a longer suspension time in fracturing fluids. However, due to their highly porous structure, ultra-low weight proppants cannot withstand high compressive

stress (Feng *et al.*, 2021). Gas-suspended proppants are complex and expensive to use in hydraulic fracturing operations.

Herein, we propose a new technique, the so-called self-generated gas floating technique, to lift proppants to the top part of fractures. It relies on the use of self-generated CO₂ bubbles. To apply this technique in the field, we plan to inject fracturing fluid with proppants and a base (sodium bicarbonate) into the wellbore during the slurry stage. Subsequently, we inject fracturing fluid with an acid (acetic acid) to initiate the acid-base reactions inside the fracture. The acid-base reactions will generate CO₂ bubbles which can potentially lift the proppants to the upper location of the fracture.

To successfully apply the self-generated gas floating technique in hydraulic fracturing operations, proppant surface wettability is an important property that needs to be considered as the interaction of gas bubbles and proppants is a critical factor in this technique. Wettability describes how easily that a liquid droplet adheres on a solid surface, and it can be quantified by measuring the contact angle of the liquid droplet on the solid surface (Abdelbary and Li, 2023). Hydrophobicity and hydrophilicity define two different types of wettability of a given solid surface with respect to water. For instance, people make umbrellas using hydrophobic materials so that umbrella can repel water more easily. The contact angle refers to the angle between the horizontal line parallel to the surface (solid/liquid interface) and the tangent line of the liquid/atmosphere interface across the three-phase contact point (Alghunaim *et al.*, 2015). The surface is water-wet if the contact angle of a water droplet on the surface is less than 90 degrees, neutral wet when the contact

angle is around 90 degrees, and gas/oil wet when the contact angle is greater than 90 degrees.

Previous studies show that hydrophobic proppants have a better performance than hydrophilic proppants. Oil-wet proppants tend to yield a higher hydrocarbon production rate and a lower water-cut (Xiao *et al.*, 2019). One advantage of oil-wet proppants is their low settling velocity. One study has investigated the settling velocity of hydrophobic FeCO₃ particles (Soames *et al.*, 2019; Yao *et al.*, 2022). The author found that the hydrophobic FeCO₃ particles settle way more slowly than surfactant-treated hydrophilic particles. Oil-wetted FeCO₃ particles attract each other and form large particle aggregates during the settling motion. Moreover, when conducting sand bed erosion experiments in a horizontal pipe, the authors observed that air bubbles can more easily attach to hydrophobic sand particles (Hipra *et al.*, 2020). The attachment of gas bubbles can provide an extra lifting force during the settlement of sand particles. Furthermore, some studies show that epoxy resin can adsorb carbon dioxide (Buijs and Flart, 2017; Yin *et al.*, 2019). This could be highly beneficial for applying the self-generated gas floating technique on resin-coated proppants since the reaction-generated CO₂ can be adsorbed by resin.

In this chapter, we first experiment with coating a layer of siliconizing fluid called SurfaSil on ceramic proppants. Three types of proppants with different surface characteristics are made available: ceramic proppants, resin-coated proppants, and SurfaSil-treated proppants. The contact angle of each type of proppants is measured. We also measured the contact angles of air/CO₂ in an aqueous environment, and we find the contact angle of CO₂ is

smaller than the contact angle of air. Besides the contact angle measurements, a fracture model that consists of two acrylic sheets is used to visually study the interaction of three types of proppants with air and reaction-generated CO₂. The influence of five variables on proppants placement efficiency is examined, including fracture width, reaction rate, surface wettability, size of proppants and type of gas bubbles. CO₂ bubbles are produced from the reaction of sodium bicarbonate (NaHCO₃) with acetic acid (CH₃COOH). Proppant placement efficiencies are quantified through image analysis. The investigated zone to be analyzed is located at the top of the fracture model. Photos of the investigated zone are taken before and after the reaction of the acetic acid with sodium bicarbonate or after the injection of air. In the investigated zone, the ratio of the area occupied by the proppants to the entire area of the investigated zone can be calculated through a MATLAB code. The ratio is called the proppant coverage ratio and can qualitatively represent the proppant placement efficiency.

2.2 Experimental Section

2.2.1 Materials

Both ceramic proppants and resin-coated proppants with intermediate strength are purchased from Henan Tianxiang New Materials Co. LTD. The proppants with mesh sizes of 16/30 and 30/50 are used in the experiments. The properties of each type of proppants are illustrated in Table 2.1. Unlike ceramic proppants, resin-coated proppants are manufactured by coating a layer of resin material on proppants. Additionally, we modify the surface wettability of ceramic proppants. SurfaSil (Thermal Scientific), which consists of mainly dichlorooctamethyltetrasiloxane, is used in the experiments as the wettability-

alteration chemical agent. To avoid the chemical reaction between resin and SurfaSil, only ceramic proppants are used to prepare for SurfaSil-treated proppants. The high-speed camera is the Chronos 1.4 Camera purchased from Kron Technologies. A KDS-250 syringe pump is purchased from KD Scientific. Transparent acrylic sheets are used to build the fracture model, and rubber sheets are required to seal the fracture model and allow us to change the fracture width.

Table 2.1 Properties of ceramic proppants and resin-coated proppants with different mesh sizes

Mesh size	16/30		30/50	
Proppant type	Ceramic proppants	Resin-coated proppants	Ceramic proppants	Resin-coated proppants
Parameter				
Apparent density (g/cm ³)	3.29	3.08	3.16	3.01
Crush Resistance (psi)	10,000	10,000	10,000	10,000
Bulk Density (g/cm ³)	1.85	1.81	1.72	1.75
Sphericity	0.86	0.86	0.86	0.87

Note: The apparent density is the mass of a particle divided by its volume; The bulk density is the mass of particles divided by their occupied volume (including the porous volume); The crush resistance defines the maximum compressive stress that a particle can withstand; The sphericity measures the shape of a particle compared with a sphere (ranges from 0 to 1).

2.2.2 Experimental setup

2.2.2.1 Setup of the SurfaSil coating experiment

Figure 2.1 demonstrates the process of wettability alteration of proppants from a water-wet surface to a gas-wet surface. Ceramic proppants are immersed in the diluted SurfaSil

solution and then rinsed with toluene and methanol. These proppants are then dried in the oven. We then obtain the SurfaSil-treated proppants. Our goal is to prepare three types of proppants with different surface wettability to investigate the influence of proppant wettability on proppant placement efficiency.

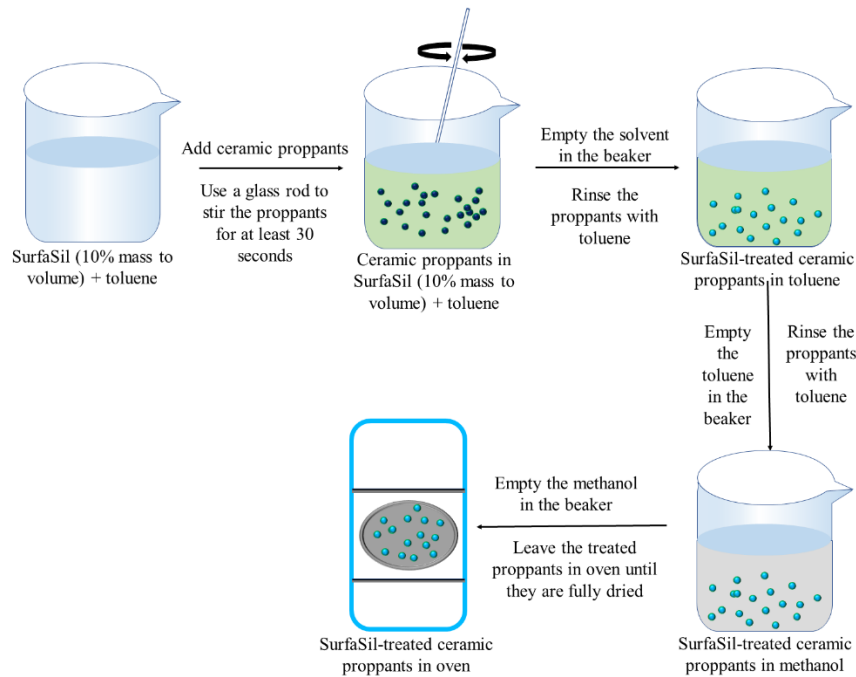


Figure 2.1 Schematic of SurfaSil coating experiment

2.2.2.2 Contact angle of a water droplet on proppants

The sessile drop method (Alghunaim *et al.*, 2015) is applied to measure the contact angles of a water droplet on ceramic proppants, resin-coated proppants and SurfaSil-treated proppants. Figure 2.2 shows the schematic of the experimental setup used for such measurements. Proppants are first glued to a plastic tape and placed on a horizontally levelled desk. The high-speed camera is then placed adjacent to the plastic tape to capture the digital images of the water droplet spreading on top of the proppants. The smallest proppants (mesh size 30/50) are used for wettability measurements. The contact angle measurements are conducted under ambient conditions.

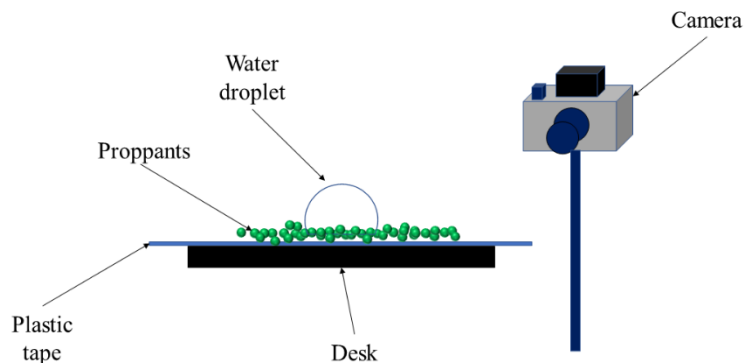


Figure 2.2 Schematic of experimental setup used to measure the contact angle of a water droplet on ceramic proppants, resin-coated proppants and SurfaSil-treated proppants

2.2.2.3 Contact angle of an air or CO₂ bubble on proppants

Figure 2.3 demonstrates the schematic of experimental setup used to measure the contact angle of an air or CO₂ bubble on resin-coated proppants under an aqueous condition. A plastic tape is floating on the water filled in a beaker. The lower side of the plastic tape that resin-coated proppants attach to is under water. CO₂ or air is injected from the bottom of the beaker, and then gas bubbles rise and attach to the resin-coated proppants layer. The Chronos high-speed camera is placed adjacent to the beaker to capture the digital images.

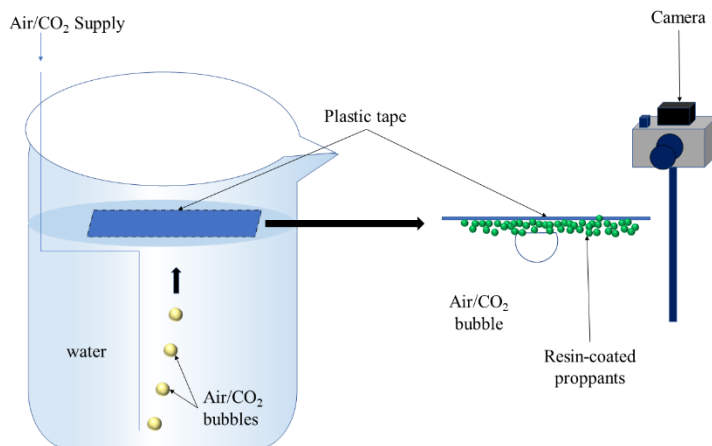


Figure 2.3 Schematic of the experimental setup used to measure the contact angle of an air or CO₂ bubble on resin-coated proppants in an aqueous condition

2.2.2.4 Adsorption of air/CO₂ bubbles onto proppants

We quantify the affinity of air/CO₂ to proppants by setting up another experiment; the corresponding schematic of the experimental setup is shown in Figure 2.4. Resin-coated proppants are placed in beakers 1 and 2, and ceramic proppants are placed in beaker 3. The amount of proppants is the same in each beaker. Air is added to beaker 1 by shaking the beaker. Acetic acid and sodium bicarbonate solution are added into beakers 2 and 3 to generate CO₂. After shaking each beaker thoroughly, we visually observe the number of gas bubbles adsorbed on proppants.

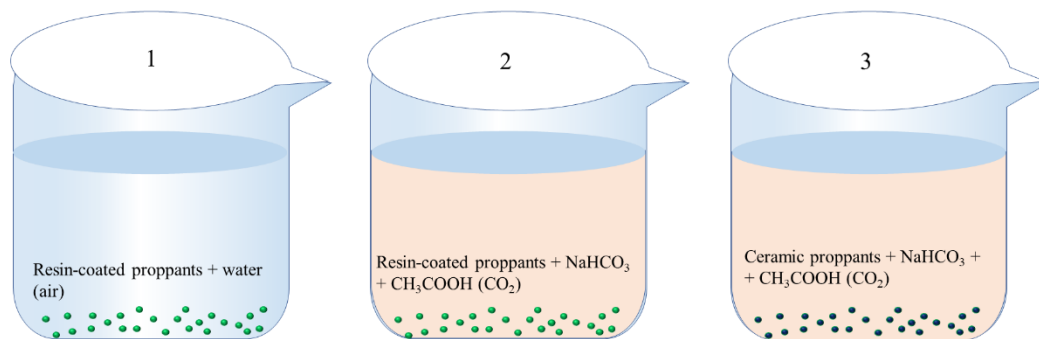


Figure 2.4 Schematic of the experiment setup used to reveal the adsorption of air/CO₂ bubbles onto proppants

2.2.2.5 Self-generated gas floating experiments

Figure 2.5 shows the schematic of the self-generated gas floating experiments. The fracture model is composed of two parallel rectangular acrylic sheets (20 × 40 cm). Rubber sheets are squeezed in between acrylic sheets. We can change the fracture width from a minimum

of 1.5 mm to a maximum of 4 mm by adjusting the number of rubber sheets in between the acrylic sheets. The air or acetic acid is injected through the inlet into the fracture model using a KD Scientific syringe pump with a maximum injection rate of 21 ml/min. Air and reaction-generated CO₂ bubbles can potentially get attached to the proppants, lifting proppants to the top of the fracture model. An investigated zone (20 × 10 cm) is set at the upper section of the fracture model to examine the proppant placement efficiency in this area. A camera is used to capture the image of the investigated zone, and the proppant placement efficiency in this investigated zone could be quantified by the proppant coverage ratio.

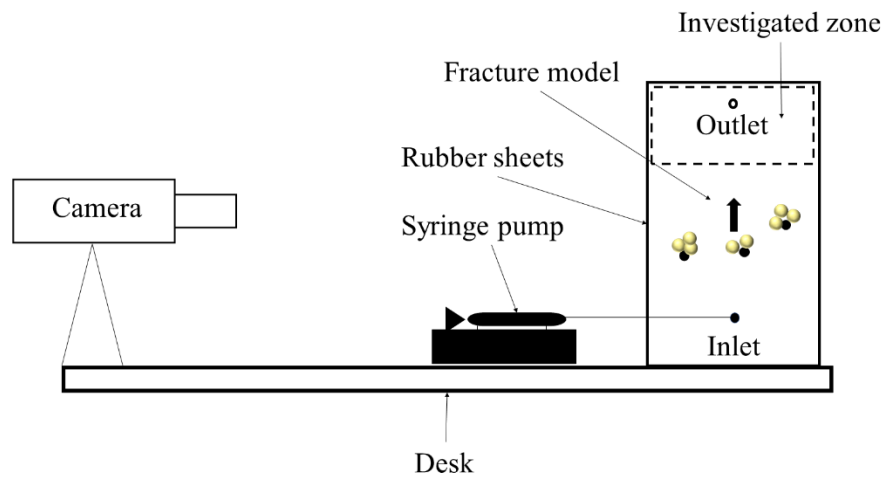


Figure 2.5 Schematic of the self-generated gas floating experiments

The objectives of the self-generated gas floating experiment is to examine the effect of proppant mesh size, proppants type, chemical reaction rate, fracture width, and type of gas bubbles (air/CO₂) on the effectiveness of the self-generated gas floating technique. The chemical reaction rate is controlled by the acid injection rate and the concentration of

sodium bicarbonate. Table 2.2 lists all experimental variables and the corresponding values.

The entire experimental schedule is listed in Table 2.3.

Table 2.2 Experimental variables and the corresponding values used in the self-generated gas floating experiments

Experimental variables	Values
Gas bubble type	CO ₂ and air
Proppant size	16/30, 30/50
Proppant type	Ceramic proppants, resin-coated proppants and SurfaSil-treated proppants
Fracture width (mm)	1.5, 4
Air and acetic acid injection rate (ml/min)	10, 21
Concentration of sodium bicarbonate (g/100 ml of water)	4, 8

Table 2.3 Experimental schedules used in the self-generated gas floating experiments

Run No.	Gas type	Injection rate (ml/min)	Concentration of sodium bicarbonate (g/100ml of water)	Type of proppant	Proppant mesh size	Fracture width (mm)
1	Air	21	N/A	Resin-coated proppants	30/50	4
2	CO ₂	21	4	Resin-coated proppants	30/50	4
3	CO ₂	10	4	Resin-coated proppants	30/50	4
4	CO ₂	10	8	Resin-coated proppants	30/50	4
5	CO ₂	21	8	Resin-coated proppants	30/50	4
6	Air	21	N/A	SurfaSil-treated proppants	30/50	4

7	CO ₂	21	4	SurfaSil-treated proppants	30/50	4
8	CO ₂	10	4	SurfaSil-treated proppants	30/50	4
9	CO ₂	10	8	SurfaSil-treated proppants	30/50	4
10	CO ₂	21	8	SurfaSil-treated proppants	30/50	4
11	Air	21	N/A	Ceramic proppants	16/30	4
12	CO ₂	21	4	Ceramic proppants	16/30	4
13	CO ₂	10	4	Ceramic proppants	16/30	4
14	CO ₂	10	8	Ceramic proppants	16/30	4
15	CO ₂	21	8	Ceramic proppants	16/30	4
16	Air	21	N/A	Resin-coated proppants	16/30	4
17	CO ₂	21	4	Resin-coated proppants	16/30	4
18	CO ₂	10	4	Resin-coated proppants	16/30	4
19	CO ₂	10	8	Resin-coated proppants	16/30	4
20	CO ₂	21	8	Resin-coated proppants	16/30	4
21	Air	21	N/A	SurfaSil-treated proppants	16/30	4
22	CO ₂	21	4	SurfaSil-treated proppants	16/30	4
23	CO ₂	10	4	SurfaSil-treated proppants	16/30	4

24	CO ₂	10	8	SurfaSil-treated proppants	16/30	4
25	CO ₂	21	8	SurfaSil-treated proppants	16/30	4
26	Air	21	N/A	Ceramic proppants	30/50	4
27	CO ₂	21	4	Ceramic proppants	30/50	4
28	CO ₂	10	4	Ceramic proppants	30/50	4
29	CO ₂	10	8	Ceramic proppants	30/50	4
30	CO ₂	21	8	Ceramic proppants	30/50	4
31	Air	21	N/A	Ceramic proppants	30/50	1.5
32	CO ₂	21	4	Ceramic proppants	30/50	1.5
33	CO ₂	10	4	Ceramic proppants	30/50	1.5
34	CO ₂	10	8	Ceramic proppants	30/50	1.5
35	CO ₂	21	8	Ceramic proppants	30/50	1.5
36	Air	21	N/A	Resin-coated proppants	30/50	1.5
37	CO ₂	21	4	Resin-coated proppants	30/50	1.5
38	CO ₂	10	4	Resin-coated proppants	30/50	1.5
39	CO ₂	10	8	Resin-coated proppants	30/50	1.5
40	CO ₂	21	8	Resin-coated proppants	30/50	1.5
41	Air	21	N/A	SurfaSil-treated proppants	30/50	1.5

42	CO ₂	21	4	SurfaSil-treated proppants	30/50	1.5
43	CO ₂	10	4	SurfaSil-treated proppants	30/50	1.5
44	CO ₂	10	8	SurfaSil-treated proppants	30/50	1.5
45	CO ₂	21	8	SurfaSil-treated proppants	30/50	1.5
46	Air	21	N/A	Ceramic proppants	16/30	1.5
47	CO ₂	21	4	Ceramic proppants	16/30	1.5
48	CO ₂	10	4	Ceramic proppants	16/30	1.5
49	CO ₂	10	8	Ceramic proppants	16/30	1.5
50	CO ₂	21	8	Ceramic proppants	16/30	1.5
51	Air	21	N/A	Resin-coated proppants	16/30	1.5
52	CO ₂	21	4	Resin-coated proppants	16/30	1.5
53	CO ₂	10	4	Resin-coated proppants	16/30	1.5
54	CO ₂	10	8	Resin-coated proppants	16/30	1.5
55	CO ₂	21	8	Resin-coated proppants	16/30	1.5
56	Air	21	N/A	SurfaSil-treated proppants	16/30	1.5
57	CO ₂	21	4	SurfaSil-treated proppants	16/30	1.5
58	CO ₂	10	4	SurfaSil-treated proppants	16/30	1.5

59	CO ₂	10	8	SurfaSil-treated proppants	16/30	1.5
60	CO ₂	21	8	SurfaSil-treated proppants	16/30	1.5

2.2.3 Experimental procedures

2.2.3.1 SurfaSil coating experiments

1. Place ceramic proppants with the mesh size of 16/30 and ceramic proppants with the mesh size of 30/50 into two beakers separately.
2. Weigh 10 grams of SurfaSil and 90 grams of toluene, and dilute the SurfaSil fluid using toluene. Thus, the SurfaSil concentration of the diluted solution is 10 % weight fraction. Put the same volume of the diluted SurfaSil solution into the two beakers with proppants.
3. Use a glass rod to stir the proppants in each beaker for at least 30 seconds to ensure SurfaSil is coated uniformly on the surface of each proppant.
4. Use a pipette to remove the SurfaSil solution in each beaker. Try to remove the solution as much as possible.
5. Add pure toluene into each beaker. Then, use the glass rod to stir the proppants. This is to rinse off the leftover SurfaSil solution on the surface of proppants.
6. Use a pipette to remove the toluene in each beaker. Try to remove the toluene as much as possible.
7. Add methanol into each beaker and use the glass rod to stir the proppants thoroughly.
8. Remove the methanol from each beaker using the pipette.
9. Repeat steps 7 and 8 for 2-3 times. Then, place the beakers with the SurfaSil-treated proppants in the vented oven until the proppants are thoroughly dried.

2.2.3.2 Contact angle of a water droplet on proppants

1. Cut three sections of plastic tape. Each section should have a length of 10 cm and a width of 5 cm.
2. Attach ceramic, resin-coated and SurfaSil-treated proppants with a mesh size of 30/50 to three plastic tapes separately, and gently press these three proppant layers to make them flat and firm.
3. Use a syringe to place a water droplet on each proppant layer.
4. Use the high-speed camera to take an image of the water droplet on each proppant layer.
5. Use an angle gauge to measure the contact angle of the water droplets on three proppant layers.

2.2.3.3 Contact angle of an air/CO₂ bubble on proppants

1. Cut three sections of plastic tape and attach each type of proppants on each section of the plastic tape.
2. Fill up a beaker with tap water and carefully float the plastic tape on the water. Make sure the proppant layer on the plastic tape is facing downward in the water.
3. Extract air/CO₂ from the atmosphere/CO₂ cylinder using a syringe. Place the outlet of the syringe at the bottom of the beaker.
4. Gently push the syringe so that air/CO₂ bubbles rise upward and touch the proppants layer.
5. Use the high-speed camera to take an image of the air/CO₂ bubble on the proppant layer.
6. Use an angle gauge to measure the contact angle of the air/CO₂ bubble on the proppant layer.

7. Repeat the same procedure for the other two types of proppants.

2.2.3.4 Adsorption of air/CO₂ bubbles onto proppants

1. Prepare three beakers and add an equal amount of resin-coated proppants with a mesh size of 30/50 into beaker 1 and beaker 2, and the same amount of ceramic proppants with a mesh size of 30/50 into beaker 3.
2. Add water and air into beaker 1. Add the sodium bicarbonate solution into beaker 2 and beaker 3. Subsequently, add the acetic acid into beaker 2 and beaker 3 to generate CO₂.
3. Seal the three beakers using a plastic wrap and shake the beakers thoroughly to ensure air/CO₂ bubbles adsorb on proppants inside the beaker.
4. Observe the amount of air/CO₂ bubbles adsorbed on proppants in each beaker.

2.2.3.5 Experimental procedure of the self-generated gas floating experiments

The experimental procedure includes two parts. The first part uses the air bubbles, and the other one uses the reaction-generated CO₂ bubbles. The corresponding procedures are listed as follows.

To examine the interaction of the proppants with air bubbles, the air is injected into the fracture model using the syringe pump. The experimental procedure of the self-generated gas floating experiment is listed as follows:

1. Add one type of proppants with a volume of 20 ml with a certain mesh size into the fracture model based on the experimental schedule.

2. Fill the fracture model with distilled water to a height of 30 cm.
3. Fill the syringe with air and connect the syringe to the inlet of the fracture model.
4. Turn on the camera and start recording.
5. Install the syringe on the syringe pump and start injecting at a specific rate based on the experimental schedule.
6. After the injection stops, pause the camera, and save the video for image analysis.
7. Disassemble the fracture model and discard the proppants.

To examine the interaction of the proppants with CO₂ bubbles, the acetic acid is injected into the fracture model filled with sodium bicarbonate solution. The experimental procedure of the self-generated gas floating experiment is listed as follows:

1. Add one type of proppants with a volume of 20 ml with a certain mesh size into the fracture model based on the experimental schedule.
2. Fill the fracture model with a certain concentration of sodium bicarbonate solution to a height of 30 cm.
3. Fill the syringe with the acetic acid and connect the syringe to the inlet of the fracture model.
4. Turn on the camera and start recording.
5. Install the syringe on the syringe pump and start injecting at a specific rate based on the experimental schedule.
6. After the reaction stops, pause the camera, and save the video for image analysis.
7. Disassemble the fracture model and discard the proppants.

After the experiments, we proceed to conduct image analysis. The image analysis is done by calculating the proppant coverage ratio in the investigated zone (20×10 cm) at the top of the fracture model. The proppant coverage ratio is equal to the proppant placement area in the investigated zone divided by the entire area of the investigated zone, which could be obtained through the MATLAB image analysis code. The difference of the proppant coverage ratio before and after the experiment is used as the final results of proppant coverage ratio in the investigated zone (R), which can be calculated as follows:

$$R = R_2 - R_1 \quad (2.1)$$

where R_2 is the proppant coverage ratio in the investigated zone after the injection process; R_1 is the proppant coverage ratio in the investigated zone before the injection process. R_1 is usually equals to zero, and we still calculate R_1 to prevent the error caused by the small number of proppants left at the investigated zone before the injection process.

Figure 2.6 and Figure 2.7 demonstrate the image analysis process from a single experiment. The rest of the processed images are listed in the Appendix of this thesis. The results of proppant coverage ratio of each experiment described in the schedule of Table 2.3 is shown in the results section.



Figure 2.6 Distribution of resin-coated proppants with a mesh size of 30/50 in the investigated zone in the 4 mm wide fracture model. The image is captured prior to the injection of acid to the fracturing fluid with 8 wt% of sodium bicarbonate. The left image is the original image, while the right one is the processed image. The proppant coverage ratio is measured to be 0.



Figure 2.7 Distribution of resin-coated proppants with a mesh size of 30/50 in the investigated zone in the 4 mm wide fracture. The image is captured post the injection of acid with the rate of 21 ml/min to the fracturing fluid with 8 wt% of sodium bicarbonate. The left image is the original image, while the right one is the processed image. The proppant coverage ratio is measured to be 0.28262.

2.3 Results and Discussion

2.3.1 Contact angle of a water droplet on proppants

The contact angles of water droplets on different proppants layers with different proppant types are shown in Figures 2.8, 2.9 and 2.10. From the contact angle measurement results, it can be seen that ceramic proppants are water-wet, resin-coated proppants and SurfaSil-treated proppants are oil-wet or gas-wet. The degree of hydrophobicity from low to high ranks as ceramic proppants, resin-coated proppants, and SurfaSil-treated proppants.

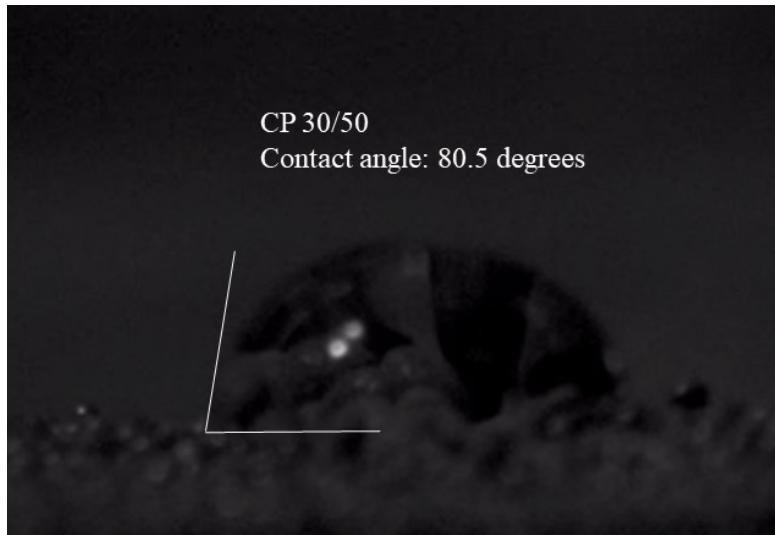


Figure 2.8 Contact angle of one water droplet on ceramic proppants with a mesh size of 30/50

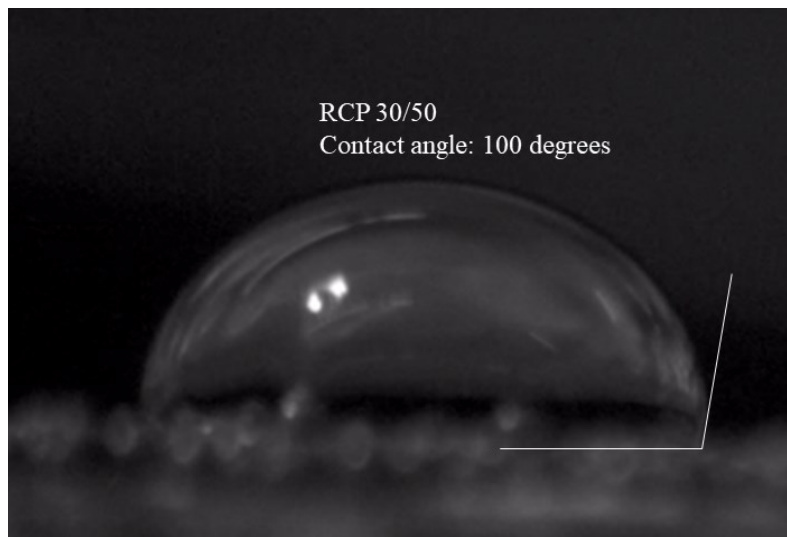


Figure 2.9 Contact angle of one water droplet on resin-coated proppants with a mesh size of 30/50

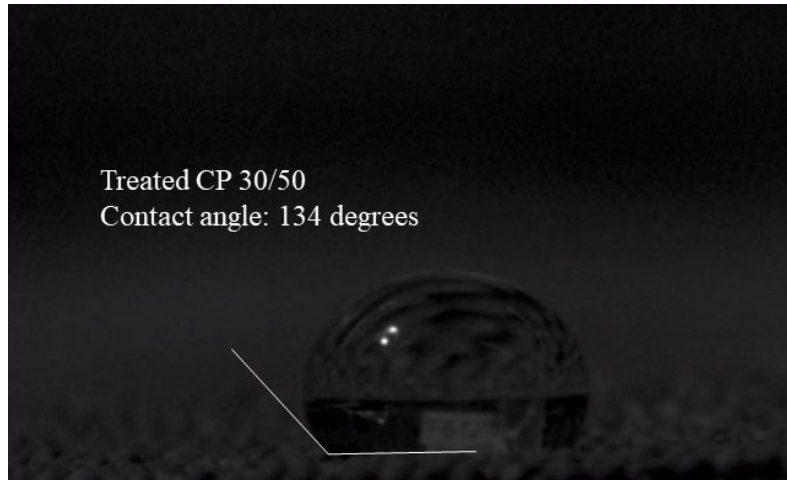


Figure 2.10 Contact angle of one water droplet on SurfaSil-treated proppants with a mesh size of 30/50

2.3.2 Contact angle of an air/CO₂ bubble on proppants

This experiment is similar to the contact angle measurement experiment of water droplets on proppant layers under the ambient condition, but the surrounding medium is changed from laboratory atmosphere to water, and the fluid medium is changed from water droplets to gas bubbles. The measurement results are shown in Figures 2.11-2.16. Based on the results of the contact angle measurements of a air bubble on each type of proppants, we can conclude that the adhesion force between air and the SurfaSil-treated proppants is the strongest, while the adhesion force between the air and the resin-coated proppants is the weakest. Based on the results of the contact angle measurements of a CO₂ bubble on each type of proppants, the contact angle of CO₂ bubble on resin-coated proppants is smaller compared to that on other type of proppants. This implies that the adhesion force between

CO₂ and resin-coated proppants is strong. Thus, CO₂ bubbles are more likely to get attached to resin-coated proppants than other types of proppants.

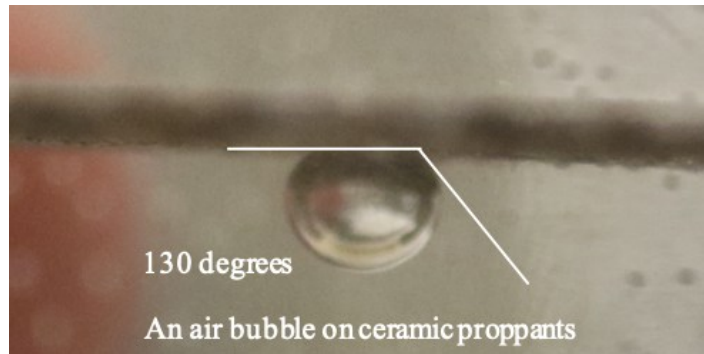


Figure 2.11 Contact angle of an air bubble on ceramic proppants in water

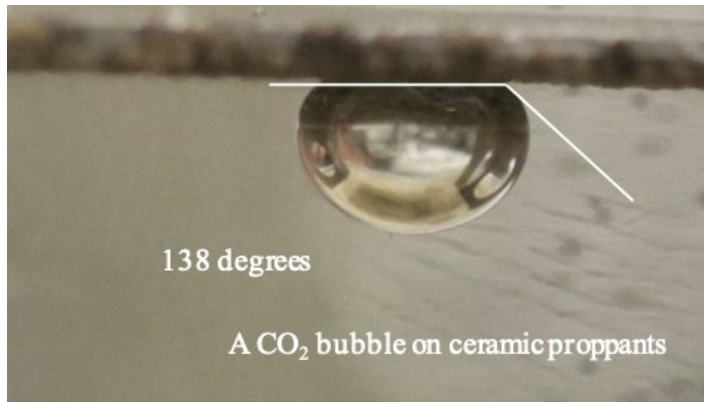


Figure 2.12 Contact angle of a CO₂ bubble on ceramic proppants in water

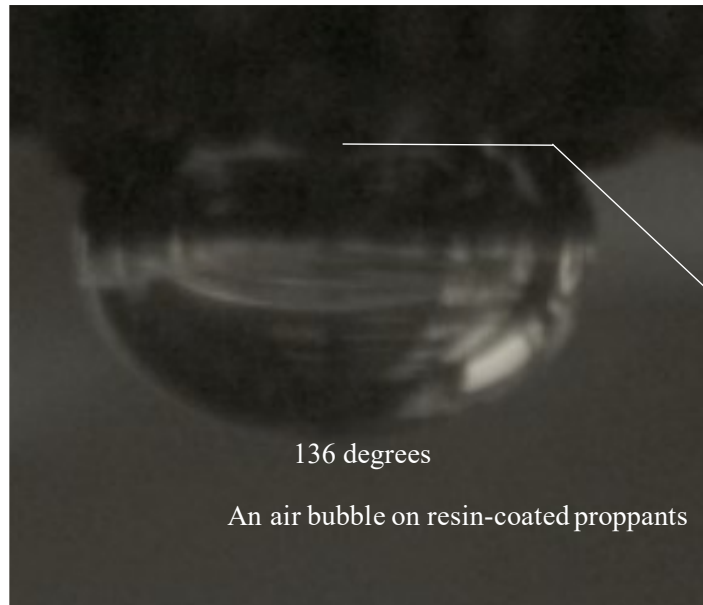


Figure 2.13 Contact angle of an air bubble on resin-coated proppants in water

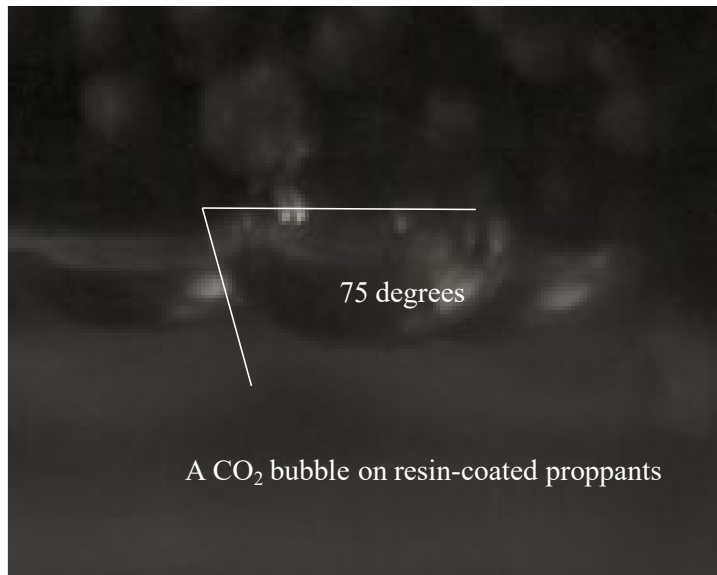


Figure 2.14 Contact angle of a CO₂ bubble on resin-coated proppants in water

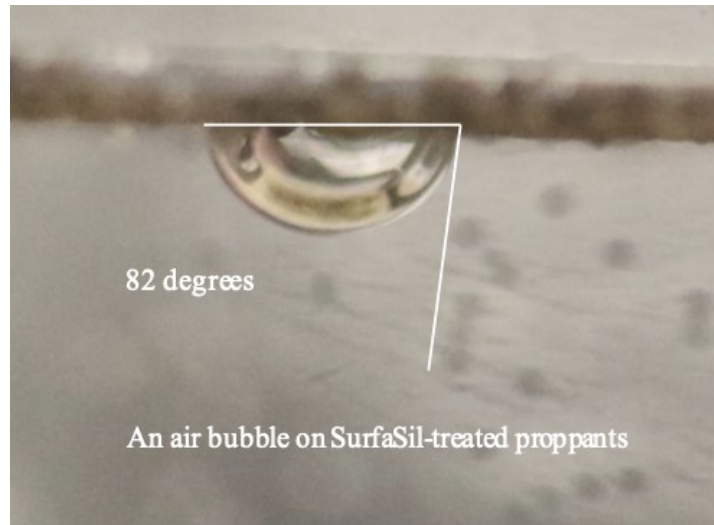


Figure 2.15 Contact angle of an air bubble on SurfaSil-treated proppants in water

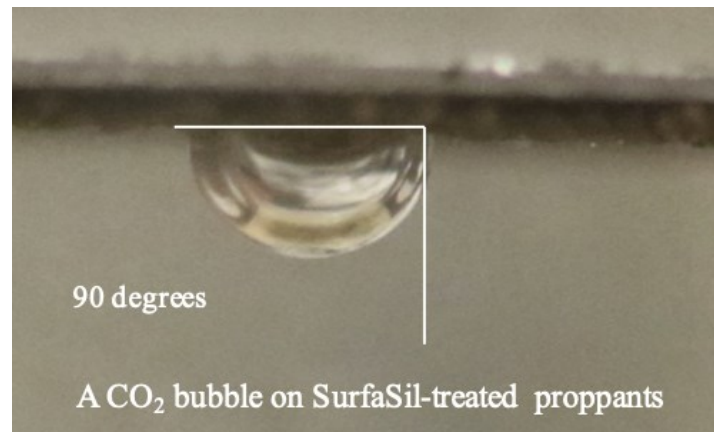


Figure 2.16 Contact angle of a CO₂ bubble on SurfaSil-treated proppants in water

2.3.3 Adsorption of air/CO₂ bubbles on proppants

To avoid the effect of an uneven proppant layer on the contact angle measurement, another visual experiment is designed to illustrate the CO₂ adsorption effect of resin coating. Figure 2.13 visually display the digital images captured after we shake the following three beakers: (a) beaker 1 is filled with resin-coated proppants and water, (b) beaker 2 is filled with resin-coated proppants and sodium bicarbonate solution, and (c) beaker 3 is filled with ceramic proppants and sodium bicarbonate solution. Acetic acid is added to beaker 2 and beaker 3 with sodium bicarbonate solution to generate CO₂. As shown in Figure 2.13 (a), there are

only a few air bubbles adsorbed onto the resin-coated proppants in beaker 1. As shown in Figure 2.13 (b), many CO₂ bubbles attach to resin-coated proppant in beaker 2, and some proppant agglomerates are floating on the surface. As shown in Figure 2.13 (c), however, CO₂ bubbles attached to ceramic proppants are less than those attached to resin-coated proppants, and all the proppants in beaker 3 settle down at the bottom of the beaker. This experiment further demonstrates that the resin-coated proppants have a higher affinity to CO₂ than air.



(a) (b) (c)
Figure 2.17 Comparison of the interaction between air/CO₂ and different proppants: (a) Resin-coated proppants with air; (b) Resin-coated proppants with CO₂; (c) Ceramic proppants with CO₂

2.3.4 Results of the self-generated gas floating experiments

The self-generated gas floating experiments are conducted to examine the effects of fracture width, proppants size, proppant type, CO₂ generation rate and gas bubble type on the effectiveness of the self-generated gas floating technique.

2.3.4.1 Effect of fracture width

The coverage ratios obtained in experiments are summarized in logarithmic plots as the coverage ratios of different types of proppants can be significantly different. The difference of coverage ratios in 4 mm fracture and 1.5 mm fracture illustrated in Figures 2.18 to 2.22 shows the influence of fracture width on the proppant placement efficiency. In these figures, CP represents ceramic proppants, RCP represents the resin-coated proppants, and TrCP represents the SurfaSil-treated proppants. The coverage ratio of each type of proppant with mesh size 30/50 in the 1.5 mm wide fracture is lower than that in the 4 mm wide fracture because of the wall effect. In the narrower fracture, the presence of the wall effect slows down the upward movement of gas bubbles and proppants. Conversely, this effect is less significant in wider fractures.

Resin-coated proppants are the proppants most significantly influenced by fracture width as they tend to aggregate and get trapped within the fracture model. Specifically, the narrower fracture prevents the aggregation of resin-coated proppants and decreases the proppant placement efficiency. In contrast, the ceramic and SurfaSil-treated proppants are less affected by fracture width due to the low proppant coverage ratio.

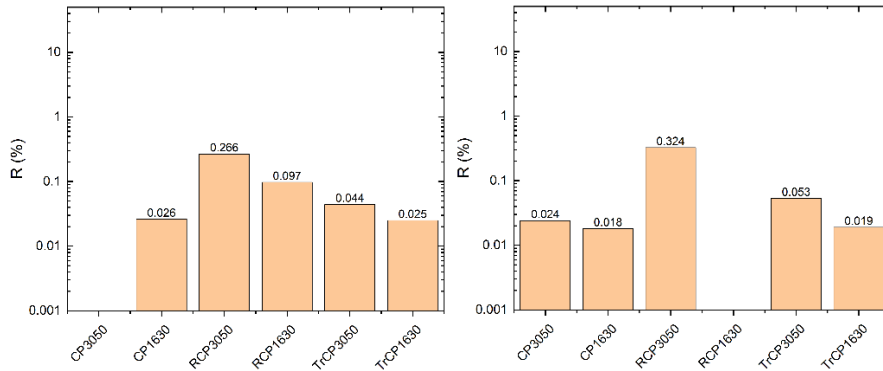


Figure 2.18 Coverage ratio of each type of proppant after air injection at a rate of 21 ml/min in the fracture model with a width of 4 mm (left) and in the fracture model with a width of 1.5 mm (right)

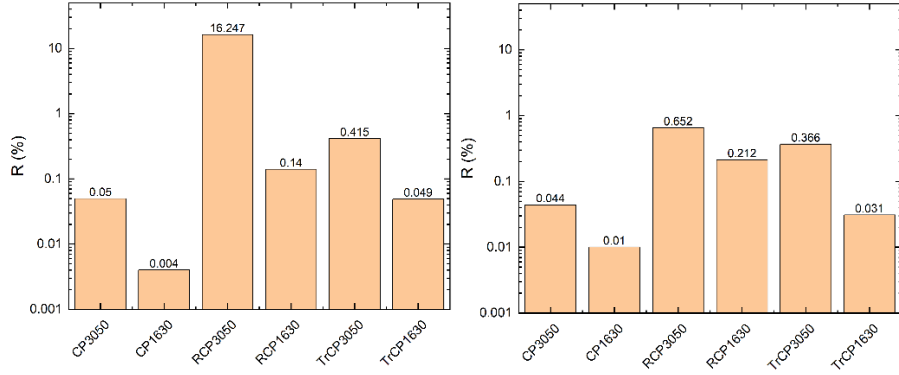


Figure 2.19 Coverage ratio of each type of proppant after the acid injection at a rate of 21 ml/min into the 4 wt% sodium bicarbonate fracturing fluid in the fracture model with a width of 4 mm (left) and in the fracture model with a width of 1.5 mm (right)

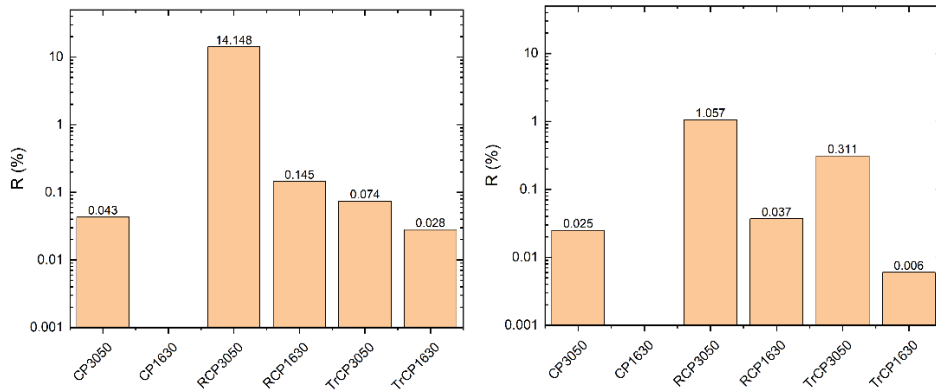


Figure 2.20 Coverage ratio of each type of proppant after the acid injection at a rate of 10 ml/min into the 4 wt% sodium bicarbonate fracturing fluid in the fracture model with a width of 4 mm (left) and in the fracture model with a width of 1.5 mm (right)

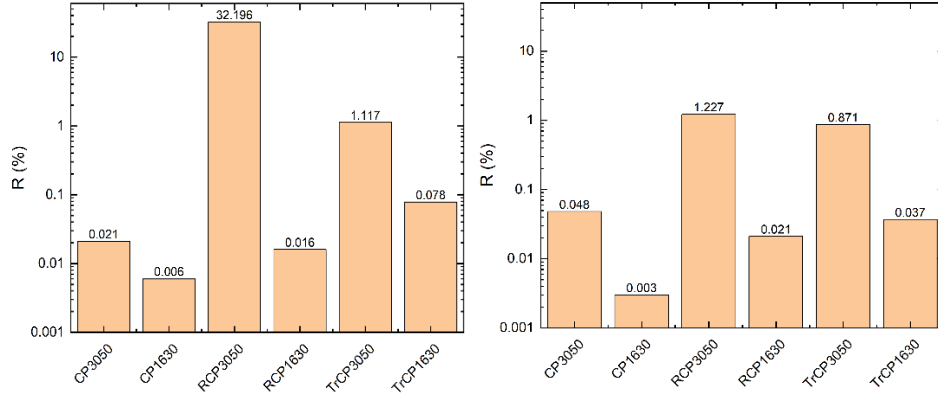


Figure 2.21 Coverage ratio of each type of proppant after the acid injection at a rate of 10 ml/min into the 8 wt% sodium bicarbonate fracturing fluid in the fracture model with a width of 4 mm (left) and in the fracture model with a width of 1.5 mm (right)

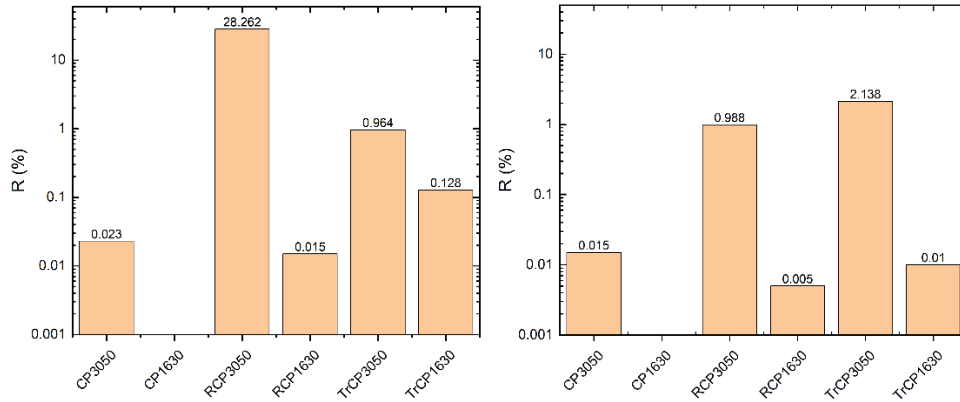


Figure 2.22 Coverage ratio of each type of proppant after the acid injection at a rate of 21 ml/min into the 8 wt% sodium bicarbonate fracturing fluid in the fracture model with a width of 4 mm (left) and in the fracture model with a width of 1.5 mm (right)

2.3.4.2 Effect of proppant size

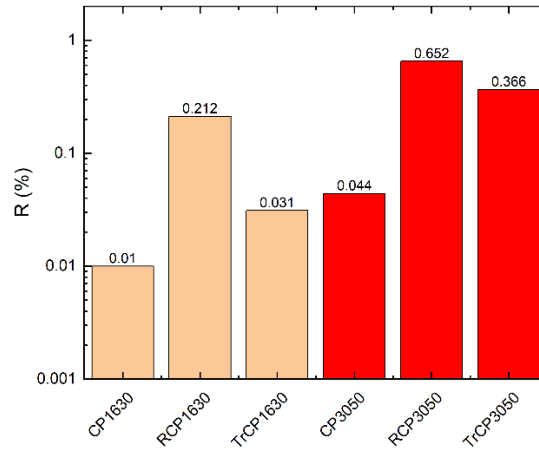


Figure 2.23 Coverage ratio of each type of proppant after the acid injection at a rate of 21 ml/min into the 4 wt% sodium bicarbonate fracturing fluid in the fracture model with a width of 1.5 mm

From Figure 2.18 to Figure 2.22, we could observe that for a given type of proppant, larger proppants (16/30 mesh size) tend to have lower or zero coverage ratios than smaller proppants (30/50 mesh size) in most cases. It can be concluded that gas bubbles cannot easily attach to larger proppants. In addition, larger proppants tend to settle down due to their higher weight. Although larger proppants occupy larger spaces in fractures, their proppant placement efficiency in the investigated zone is still low. To apply the self-generated gas floating technique in the actual hydraulic fracturing operations, it is recommended to use small-size proppants as they are more easily adsorbed by gas bubbles and more difficult to be crushed under in-situ stresses. For a more illustrative purpose, the coverage ratios shown in Figure 2.23 are rearranged from the results shown in Figure 2.19. The red bars are coverage ratios of smaller proppants (30/50 mesh size) and the incarnadine bars are the coverage ratios of larger proppants (16/30 mesh size). When the proppant type is fixed, larger proppants usually exhibit a lower proppant placement efficiency.

2.3.4.3 Effect of proppant type

From Figure 2.18 to 2.22, it can be seen that proppant type can significantly influence the proppant coverage ratio in the investigated zone. By comparing the coverage ratio of ceramic proppants and Surfasil-treated proppants with the same mesh size, the SurfaSil-treated proppants always provide a better coverage ratio. A proportional relationship between the proppant surface hydrophobicity and the proppant coverage ratio could be obtained based on the experimental results. Additionally, resin-coated proppants with a mesh size of 30/50 usually provide the highest proppant placement ratio under different situations. When being immersed in water, resin-coated proppants tend to aggregate. Gas bubbles can bring a group of resin-coated proppant aggregates instead of a small number of proppants, therefore increasing the coverage ratio. Moreover, another reason why resin-coated proppants exhibit the highest coverage ratio is the strong adhesion force between resin-coated proppants and CO₂. Based on the experimental results, we conclude that resin-coated proppants are the most suitable proppants to be used when applying the self-generated gas floating technique.

2.3.4.4 Effect of CO₂ generation rate

The rate of acid injection and the concentration of sodium bicarbonate are two variables that can affect the CO₂ generation rate. Figures 2.18 to 2.22 indicate that under the low sodium bicarbonate concentration and the low acid injection rate, the CO₂ generation rate is low, leading to a lower proppant placement efficiency. Generally, higher coverage ratios are achieved under the condition of the high acid injection rate (21 ml/min) and the high concentration of sodium bicarbonate (8 wt%).

Unlike air injection, the reaction of the sodium bicarbonate and the acetic acid produces a wide range of CO₂ bubble sizes due to the nature of the chemical reactions. The range of the generated bubble size plays a vital role in increasing the proppant coverage ratio. Figure 2.24 presents the interaction of resin-coated proppants with reaction-generated CO₂. This image demonstrates that large CO₂ bubbles possess a stronger ability to push proppants upward from the proppant bed and maximize the contact area between gas bubbles and proppants. The in-situ produced CO₂ provides the kinetic energy to push proppants to the investigated zone. Meanwhile, abundant tiny bubbles attach and bring proppants to the top of the fracture model. In this process, chemical effect (wettability) and mechanical forces are simultaneously present to increase the proppant placement efficiency.

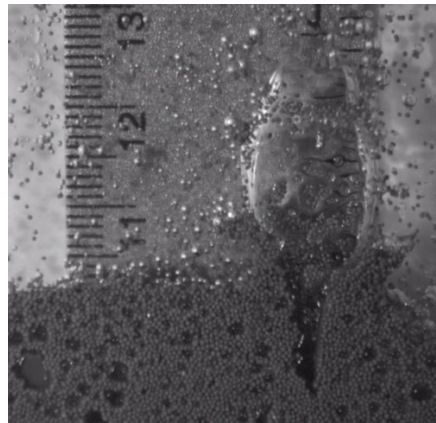


Figure 2.24 Interaction of resin-coated proppants with reaction-generated CO₂

2.3.4.5 Effect of gas bubble type

Figure 2.25 shows the coverage ratio of each type of proppant after air injection at a rate of 21 ml/min in the fracture model with a width of 4 mm (left) and the coverage ratio of each type of proppant after the acid injection at a rate of 10 ml/min into the 4 wt% of sodium bicarbonate fracturing fluid in the fracture model with a width of 4 mm (right). From Figure 2.25, even though the CO₂ generation rate is difficult to determine from the

acid injection rate, it still gives us a general idea that the proppant coverage ratio of using the reaction-generated CO₂ bubbles is significantly higher than the coverage ratio using the injected air bubbles. During the process of air injection, most proppants slide off from air bubbles, and only a few proppants attach to air bubbles and stay at the investigated zone. The mechanical pushing force dominates during the air injection process. Overall, in terms of the proppant coverage ratio, the reason why air is less efficient compared to the reaction-generated CO₂ is the slow injection rate and the weak adsorption effect of air on proppants. We could conclude that using the reaction-generated CO₂ is more beneficial to increase the proppant coverage ratio than using air.

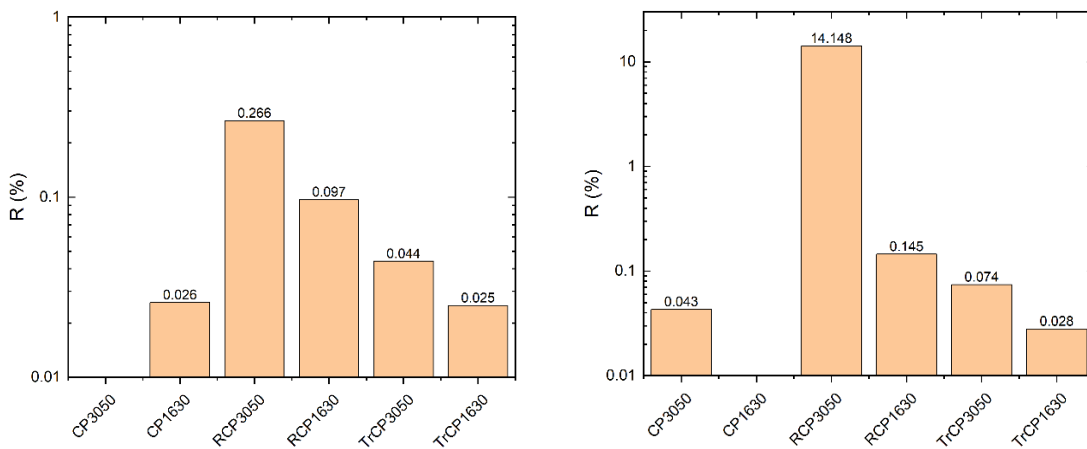


Figure 2.25 Coverage ratio of each type of proppant after air injection at a rate of 21 ml/min in the fracture model with a width of 4 mm (left) and coverage ratio of each type of proppant after the acid injection at a rate of 10 ml/min into the 4 wt% of sodium bicarbonate fracturing fluid in the fracture model with a width of 4 mm (right)

2.3.4.6 Effect of the contact angle of a CO₂ bubble on proppants

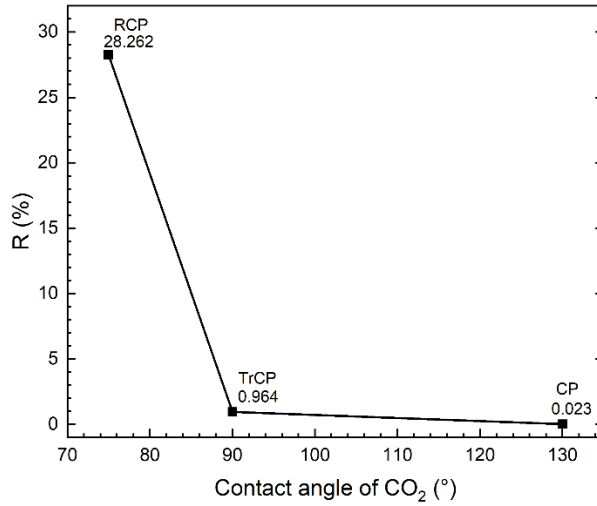


Figure 2.26 Coverage ratio of each type of proppant with the mesh size of 30/50 after the acid injection at a rate of 21 ml/min into the 8 wt% sodium bicarbonate fracturing fluid in the fracture model with a width of 4 mm versus the contact angle of a CO₂ bubble on each type of proppant

Figure 2.26 shows the relationship between the coverage ratio of each type of proppant with the mesh size of 30/50 after the acid injection at a rate of 21 ml/min into the 8 wt% sodium bicarbonate fracturing fluid in the fracture model with a width of 4 mm and the contact angle of a CO₂ bubble on each type of proppant. From Figure 2.26, we can observe an inverse relationship between the coverage ratio of each type of proppant and the CO₂ contact angle. Ceramic proppants exhibit the lowest coverage ratio and resin-coated proppants exhibit the highest coverage ratio. In addition, based on the results described in Section 2.3.2, the contact angle of the CO₂ bubble on ceramic proppants appears to be the highest while the contact angle of the CO₂ bubble on resin-coated proppants is the lowest. A higher contact angle of a CO₂ bubble on proppants implies there is a lower adhesion force between CO₂ and proppants. Thus, we can conclude that as the adhesion force between CO₂ and proppants increases, the proppants' coverage ratio also increases when using CO₂ to lift proppants.

2.4 Conclusions

In this chapter, we conduct a series of experiments to investigate how the major influential factors affect the the proppant placement efficiency yielded by the the self-generated gas floating technique. We quantify the proppant placement efficiency through the image analysis via a MATLAB code. Based on the results of these experiments, the findings can be concluded as follows:

1. The SurfaSil-treated proppants are the most hydrophobic proppants, and ceramic proppants are the most hydrophilic proppants.
2. There is a strong adsorption effect of CO₂ on resin-coated proppants. The adhesion force between resin-coated proppants and CO₂ is significantly greater than that between resin-coated proppants and air.
3. The coverage ratio of proppants in the 1.5 mm wide fracture is lower than that in the 4 mm wide fracture because of the wall effect. The fracture wall prevents the formation of proppant aggregates and slows down the upward motion of proppants and gas bubbles.
4. The proppant coverage ratio decreases with the increase of proppants size. The larger proppants are heavier than the smaller proppants, making it harder for gas bubbles to attach and bring them up.
5. By comparing the proppant coverage ratios of ceramic proppants and SurfaSil-treated proppants, we find that proppant placement efficiency increases as the hydrophobicity of the proppant surface increases. Additionally, the proppant coverage ratios of resin-coated proppants are significantly higher than those of other types of proppants due to the aggregation of resin-coated proppants when being immersed in water and the strong adhesion force between CO₂ and resin-coated proppants.

6. The proppant coverage ratios are increased significantly by a higher CO₂ generation rate. Large CO₂ bubbles possess a stronger ability to push proppants upward from the proppant bed, and abundant tiny bubbles attach and bring proppants to the top of the fracture model.

References

- Abdelbary, A., Li, C. 2023. Principles of Engineering Tribology. *Academic Press*.
- Alghunaim, A., Kirdponpattara, S., Newby, Z. B. M. 2016. Techniques for determining contact angle and wettability of powders. *Powder Technology*, 287: 201-215.
- Buijs, W., Flart, S. 2017. Direct air capture of co₂ with an amine resin: a molecular modeling study of the co₂ capturing process. *Industrial & Engineering Chemistry Research*, 56(43): 12297-12304.
- Feng, Y. C., Ma, C. Y., Deng, J. G., Li, X. R., Chu, M. M., Hui, C., Luo, Y. Y. 2021. A comprehensive review of ultralow-weight proppant technology. *Petroleum Science*, 18: 807-826.
- Hirpa, M. M., Arnipally, S. K., Bizhani, M., Kuru, E., Gelves, G., Al-Rafia, I. 2020. Effect of particle size and surface properties on the sandbed erosion with water flow in a horizontal pipe. *SPE Journal*, 25(03): 1096-1112.
- Soames, A., Al-Anssari, S., Iglauer, S., Barifcani, A., Gubner, R. 2019. Effect of wettability on particle settlement behavior within Mono-Ethylene Glycol regeneration pre-treatment systems. *Journal of Petroleum Science and Engineering*, 179: 831-840.

- Wang, J., Elsworth, D. 2018. Role of proppant distribution on the evolution of hydraulic fracture conductivity. *Journal of Petroleum Science and Engineering*, 166: 249-262.
- Xiao, D., Wang, M., Guo, B., Weng, D. 2019. Effect of surface wetting behavior of ceramic proppant on the two-phase flow across the interface of sandstone and fracture. *Energy Science & Engineering*, 8(4): 1330-1336.
- Yao, S., Chang, C., Hai, K., Huang, H., Li, H. 2022. A review of experimental studies on the proppant settling in hydraulic fractures. *Journal of Petroleum Science and Engineering*, 208: 109211.
- Yin, Y. B., Yang, Q. S., Wang, S. L., Gao, H. D., He, Y. W., Li, X. L. 2019. Formation of CO₂ bubbles in epoxy resin coatings: a DFT study. *Journal of Molecular Graphics and Modelling*, 86: 192-198.

Chapter 3: A Visual Experimental Study: The Application of the Self-generated Gas Floating Technique under Reservoir Conditions

3.1 Introduction

Hydraulic fracturing operation is a well stimulation method that aims to recover hydrocarbons from conventional and tight formations (Saunders, 2019). Hydraulic fracturing involves injecting high-pressure fracturing fluid into the perforations to crack reservoir rock and induce fractures to increase fracture conductivity (Khan *et al.*, 2021) (which measures the ability of hydrocarbon to flow into the wellbore through the propped fracture (Ma *et al.*, 2016)). There are usually three stages in a hydraulic fracturing operation, including the pad stage, the slurry stage and the completion stage (Shojaei and Shao, 2017). The pad stage includes the injection of high-pressure fracturing fluid to crack formation and generate fractures. The slurry stage involves the injection of the mixture of proppants and fracturing fluid from the surface. After the slurry stage, the completion stage ensues. The completion stage involves the flow back of a small amount of the fracturing fluid. The pump stops running and the bottomhole pressure declines significantly, further leading to a rapid reduction in the wellhead pressure as seen from Figure 3.1. The rapid decline of bottomhole pressure is mainly caused by the disappearance of frictional pressure drop and leak-off of fracturing fluid into formations (Wang *et al.*, 2021; Guo *et al.*, 2007). The high pressure decline rate may be favourable as it may be able to increase the intensity of the base-acid reactions in the self-generated gas floating technique, thereby helping increase the proppant placement efficiency. It is important to get a general understanding of how

fast the pressure can decline during the completion stage of actual hydraulic fracturing operations.

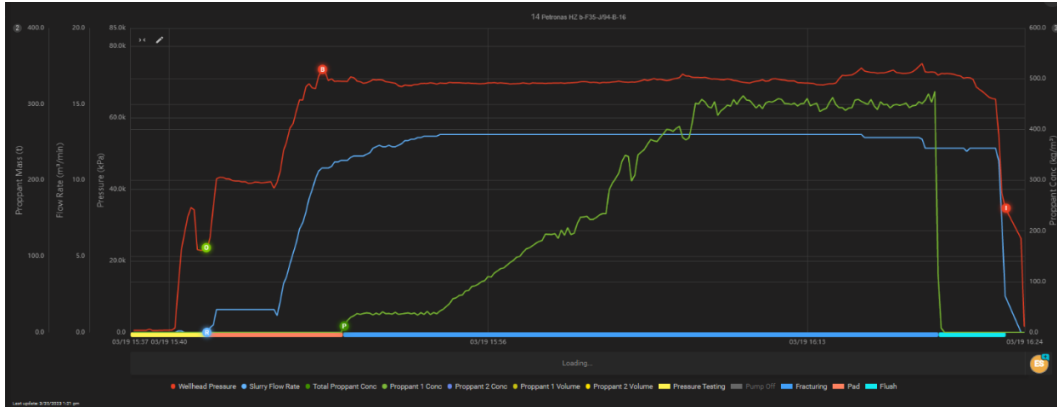


Figure 3.1 Hydraulic-fracturing field data provided by PETRONAS Canada

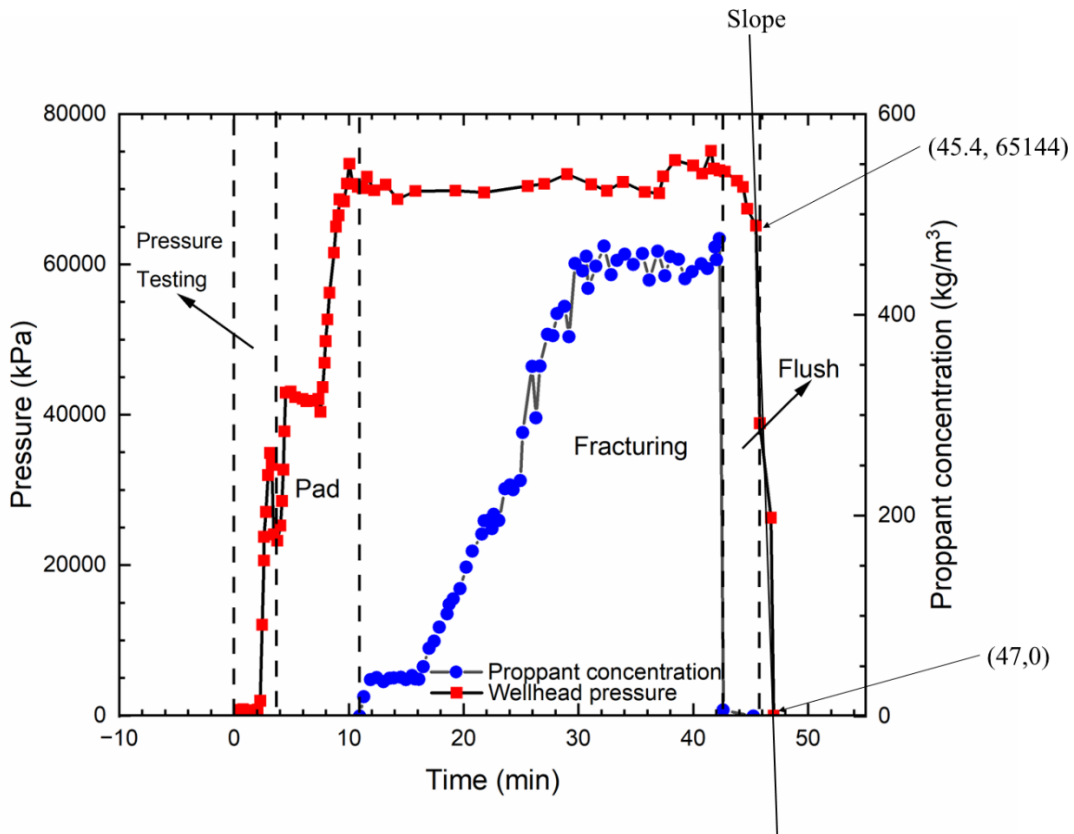


Figure 3.2 Retrieved pressure data from a hydraulic fracturing operation done by PETRONAS Canada

Figure 3.2 shows a clearer picture of the hydraulic-fracturing pressure data appearing in Figure 3.1. The red line represents the recorded wellhead pressure, while the blue line represents the proppant concentration. Before the start of the hydraulic fracturing operation, it is important to check for leakage of the entire pressure system, and this period is called the pressure testing stage. During the pad stage, pure fracturing fluid is injected into the wellbore to induce fractures. The wellhead pressure, as represented by the red line, fluctuates and eventually increases to a climax of 75 MPa. The pressure on the climax indicates the rocks are broken down and it is called breakdown pressure (Detournay and Carbonell, 1997). However, these fractures are not mature and need further propagation. Thus, the slurry stage ensues. There is no significant wellhead pressure variation as fractures keep propagating during the slurry stage. After the induced fractures have grown to a desired length, proppant injection stops and the slurry stage ends. In this case, there is an additional flush stage after the slurry stage. The implementation of the flush stage is to wash off excessive proppants left in the wellbore (Belyadi *et al.*, 2019). The flush stage is followed by the completion stage. During the completion stage, pumps stop running and the flowback of fracturing fluid happens. One thing worth noticing is that the wellhead pressure decreases significantly during the completion stage. The pressure decline rate (m) reaches 42 MPa per minute:

$$m = \frac{(65144-0)\text{MPa}}{(47-45.4487)\text{min}} = 42 \text{ MPa/min} \quad (3.1)$$

Proppant placement is the most critical part of hydraulic fracturing as proppant keeps fractures open and maintains the fracture conductivity. However, fracture conductivity can also be decreased due to the improper use of proppants. For instance, low-strength proppants tend to be crushed under formations with high in-situ stresses. The crushed

proppant debris decreases the permeability of the proppant bed (Bandara *et al.*, 2021). In addition, proppants tend to settle down inside fractures due to the gravitational force, leaving the upper part of fractures unpropped. The unpropped fractures tend to close and result in the reduction of fracture conductivity (Mehmood *et al.*, 2021). Overall, maximizing the proppant placement efficiency in the upper part of fractures is crucial for maintaining optimal reservoir conductivity.

There are many experiments conducted in the past to increase proppants placement efficiency in the upper part of fractures. Researchers develop new proppants such as ultra-low weight proppants and hydrogel-coated proppants to prolong the proppant suspension time in the fracturing fluid. Gas-suspended proppants technique is also developed; it injects nitrogen to attach and bring the hydrophobic proppants to the upper sections of fractures. The applications of these proppant technologies often yield two common issues: high costs and elevated complexity. In this study, we propose the so-called self-generated gas floating technique to mitigate these issues while increasing the proppant placement efficiency. This technique utilizes the reaction-generated CO₂ to lift proppants to the upper sections of fractures. Based on our experimental results, the procedure of the field implementation of the self-generated gas floating technique can be executed with the following procedure:

1. Mix sodium bicarbonate and proppants in the fracturing fluid and inject the mixture during the slurry stage.
2. Subsequently, mix acetic acid and proppants in the fracturing fluid and inject the mixture a few minutes before the end of the slurry stage.
3. After pumping, the sudden decline of wellbore pressure will initiate the acid-base reactions and release CO₂ bubbles, bringing the proppants upward inside fractures.

Chapter 3 covers the experiments conducted in the laboratory to simulate the application of the self-generated gas floating technique under reservoir conditions during the completion stage of the hydraulic fracturing operation. Resin-coated proppants are utilized as they exhibit the highest proppant placement efficiency in the fracture model, as proven in Chapter 2. During the completion stage, the disappearance of the frictional pressure drop in the completion stage causes a significant decrease of the bottomhole pressure. To study the effect of the pressure decline rate on the proppant placement efficiency, two different pressure decline rates (0.69 MPa/min and 5 MPa/min) are selected. We plan to apply the self-generated gas floating technique in a high-pressure reactor. Resin-coated proppants with 8 wt% of sodium bicarbonate are first placed in the reactor. A CO₂ cylinder is used to pressurize the reactor. After the pressure in the reactor reaches the desired pressure, acetic acid is subsequently injected into the reactor. The entire pressure drawdown process in the reactor is recorded, and attention is paid towards the movement of proppants inside the reactor.

3.2 Experimental Section

3.2.1 Materials

The proppant type used in this experiment is resin-coated proppant with a mesh size of 30/50 (Henan Tianxiang New Materials Co. LTD). The properties of resin-coated proppants are listed in Table 3.1.

Table 3.1 Properties of resin-coated proppants with mesh size 30/50

Parameter	Resin-Coated proppants
Apparent Density (g/cm ³)	3.01

Crush Resistance (psi)	10,000
Bulk density (g/cm ³)	1.75
Sphericity	0.87

3.2.2 Experimental setup

The experimental system is mainly made of a TELEDYNE D-Series Syringe ISCO pump, an explosion-proof oven, a high-pressure reactor, a CO₂ cylinder, and two high-pressure accumulators. The maximum operating pressure of the high-pressure reactor is 50 MPa. There is a piston in each accumulator that can move up and down. Sodium bicarbonate solution and resin-coated proppants are first placed into the reactor before the start of the experiment. The reactor is heated by an oven. A CO₂ cylinder is used to pressurize the reactor. There is a three-way bleed valve that allows us to bleed the entire system. ISCO pumps are filled with water, so the piston in the accumulator 1 is pushed up by ISCO Pump 1 to pressurize the CO₂ above the piston. The pressure gauge measures the CO₂ pressure in the entire system. Acetic acid in accumulator 2 is then injected by ISCO Pump 2 into the reactor after the pressure reaches 10 MPa. Then, we decrease the pressure at different decline rates to simulate pressure variations occurring at the completion stage of hydraulic fracturing. The entire process is recorded by an iPhone camera. Table 3.2 lists the experimental parameters used in the high-pressure experiments.

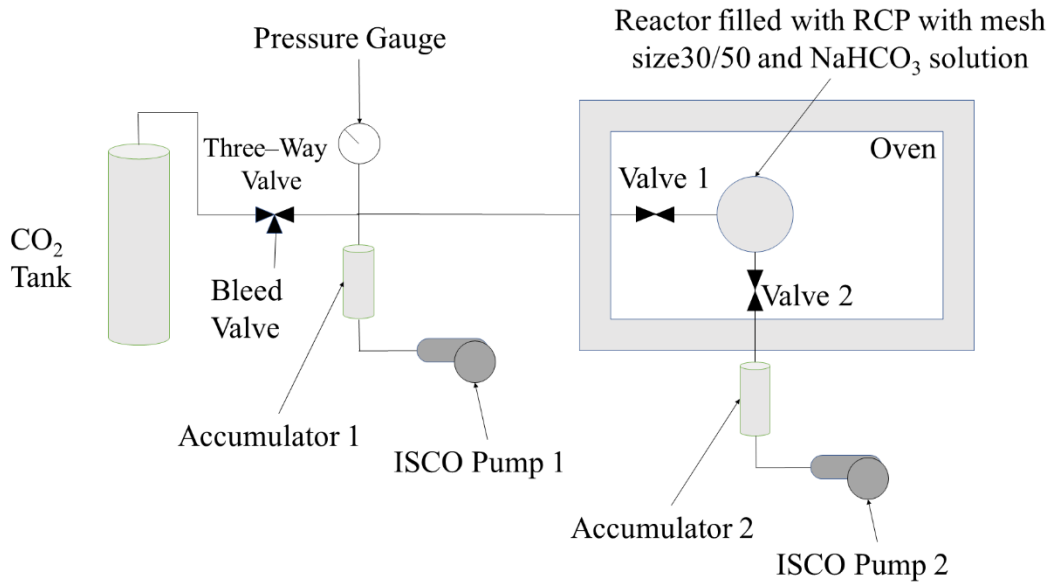


Figure 3.3 Schematic showing the experimental setup used to conduct the self-generated gas floating experiment under high-pressure conditions

Table 3.2 Experimental parameters of the high-pressure experiments

Experimental variables	Values
Acid injection pressure (Controlled by ISCO pump 2)	14.5 MPa
Temperature in the reactor	38 degrees Celsius
Pressure in the reactor	10 MPa
Concentration of NaHCO ₃	8 wt%
CO ₂ compression pressure in accumulator 1 (controlled by ISCO pump 1)	10 MPa
Pressure decline rates (During the completion stage)	0.69 MPa/min and 5 MPa/min

3.2.3 Experimental procedure

1. Turn on the oven, and heat the high-pressure reactor to 38°C.
2. Fill the reactor with a fracturing fluid with 8 wt% of NaHCO₃ and 20 ml resin-coated proppants with a mesh size 30/50. Close the three-way valve and valves 1 and 2. Set up the camera and start recording.
3. Ensure the piston inside the accumulator that connects ISCO Pump 1 is at the bottom. If no, refill ISCO pump 1 to withdraw water inside accumulator 1. Fill accumulator 2 with acetic acid.
4. Open the valve of the CO₂ cylinder and open the three-way valve to fill accumulator 1 with CO₂.
5. Close the three-way valve and control the ISCO pump 1 to pressurize the CO₂ in the accumulator to 10 MPa.
6. Open valve 1 to send the pressurized CO₂ to the reactor.
7. Check the pressure gauge to make sure the reading is at 10 MPa. If not, close the valve 1 and refill the pump with water in the accumulator. Thus, the piston goes down. Then, repeat steps from 3 to 5 until the pressure in the reactor reaches 10 MPa.
8. Close valve 1. Operate ISCO Pump 2 to inject the acetic acid into the reactor with an injection pressure of 14.5 MPa. Open valve 2 at the same time. After the pressure in the reactor reaches 14.5 MPa, stop acid injection.
9. Open valve 1 and the bleed valve, and bleed the pressure in the reactor to 10 MPa. Close valve 1.
10. On ISCO pump 1, control the pump to withdraw the water to achieve a pressure decrease rate of 0.69 psi/min. Repeat steps 1 to 8 and decrease the pressure at a rate of


5 MPa/min. Record and compare the phenomena in the reactor during the process of the pressure decline. Bleed the entire system after the experiment.

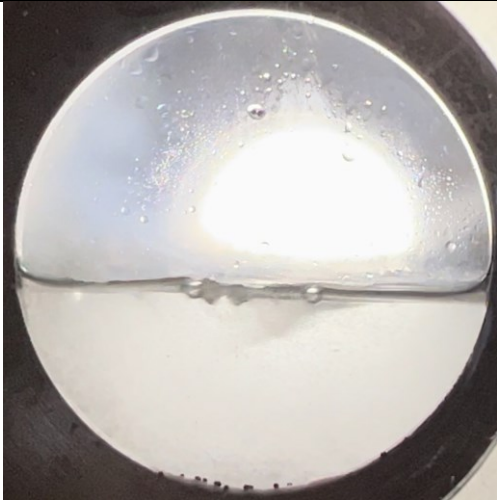
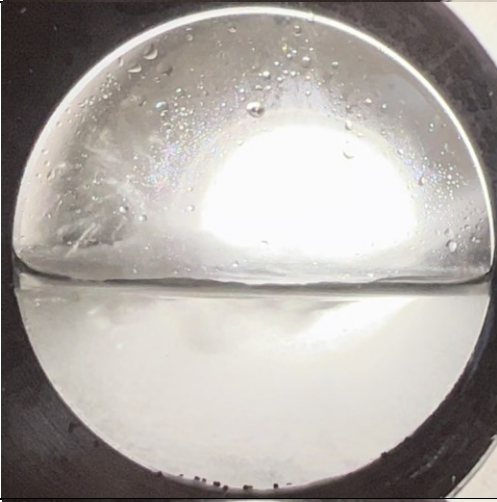
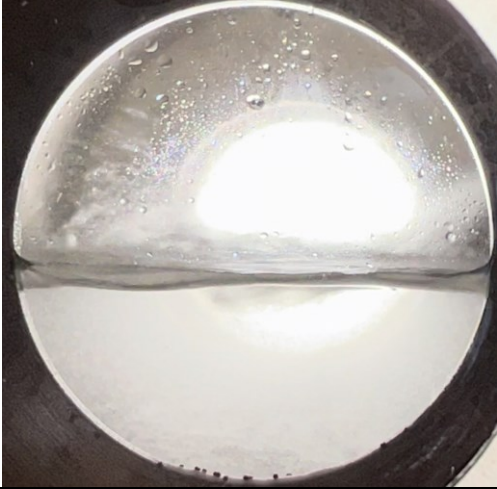
3.3 Results and Discussion




In this section, we discuss the observations and findings made based on the high-pressure experiments. We pay special attention to the effect of pressure decline rates on the lifting of proppants to the upper location of the reactor.

3.3.1 Pressurization of the reactor using CO₂

Figure 3.4 shows the images of the inner reactor captured during the pressurization of the reactor using CO₂. From Figure 3.4, we can see that CO₂ enters the reactor and forms a liquid layer above the sodium bicarbonate solution. The CO₂ layer keeps rising until all CO₂ in the gas phase turns into the liquid phase. It can be seen that there is no observation of significant proppant motion when pressurizing the reactor using CO₂.

Time, s	The images of the inner reactor during the process of pressurizing the reactor
10	

20		 A circular micrograph showing a spherical droplet on a dark surface. The droplet is highly reflective, with a bright central spot and a dark, shadowed lower half. The surface of the droplet is covered with small, clear water droplets. The background is dark and textured.	
30		 A circular micrograph showing a spherical droplet on a dark surface. The droplet is highly reflective, with a bright central spot and a dark, shadowed lower half. The surface of the droplet is covered with small, clear water droplets. The background is dark and textured.	
40		 A circular micrograph showing a spherical droplet on a dark surface. The droplet is highly reflective, with a bright central spot and a dark, shadowed lower half. The surface of the droplet is covered with small, clear water droplets. The background is dark and textured.	

50		 A circular cross-section of a spherical droplet, likely on a dark surface. The droplet is partially filled with a white, opaque substance. The upper half is clear, showing the curved surface of the droplet and some condensation droplets on the surrounding surface. The lower half is filled with the white substance, which appears to be a solid or a very thick liquid. The interface between the clear and white regions is a distinct horizontal line.	
60		 A circular cross-section of a spherical droplet, similar to the one above. The white substance is more spread out and appears slightly more granular. The clear upper portion is still visible, and the horizontal interface line is present.	
70		 A circular cross-section of a spherical droplet. The white substance is more dispersed and appears as a thin, irregular layer. The clear upper portion is still visible, and the horizontal interface line is present.	

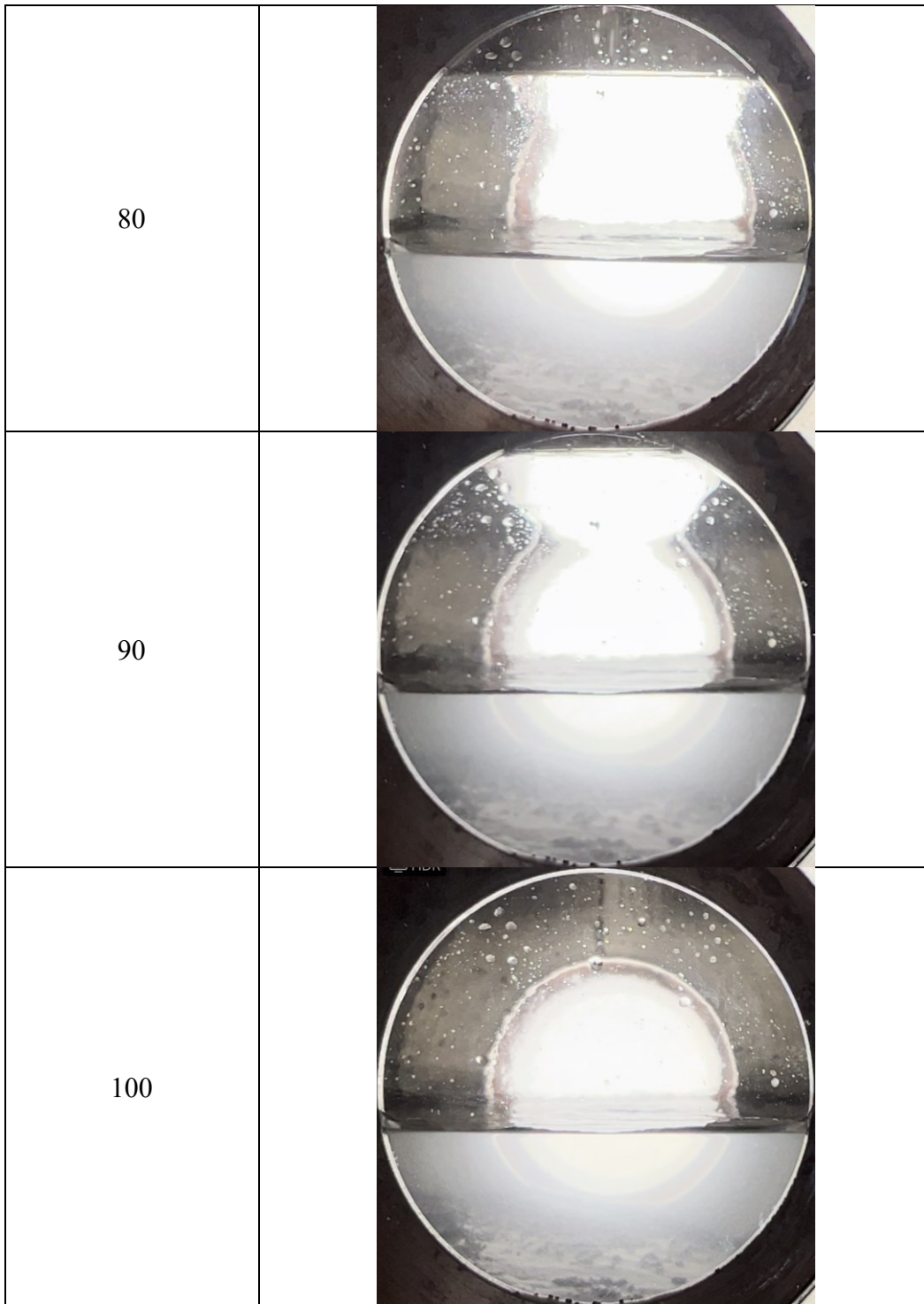




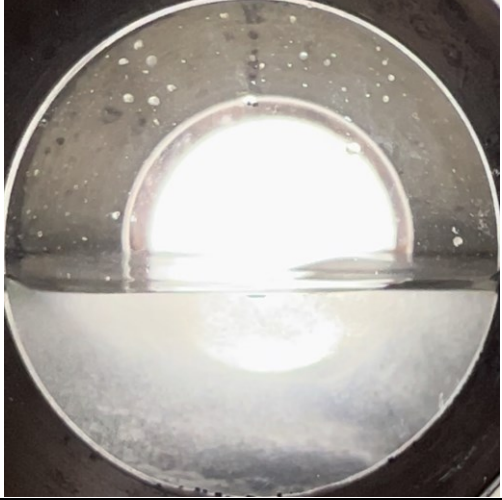


Figure 3.4 Images captured during the process of pressurizing the reactor

3.3.2 Acid injection process

The acetic acid is injected into the reactor after the pressure reaches 10 MPa. We set the injection pressure to 14.5 MPa on ISCO pump 2. The injection pressure should be higher than the pressure in the reactor to ensure enough acid is injected into the reactor. Acetic acid is a nearly incompressible fluid which can increase the pressure in the reactor substantially. The injection process stops when the pressure in the reactor reaches 14.5 MPa. . Figure 3.5 shows the process of acid injection into the reactor.

Time (s)	The images of the inner reactor during the process of acid injection (acid injection pressure: 14.5 MPa)	
5		
10		

15		 A circular structure, possibly a cell or microorganism, is shown in a dark field. The structure is roughly circular with a bright, glowing center. The outer boundary is slightly irregular and appears to have some internal structure or texture. The background is dark with some faint, scattered light spots.	
20		 A circular structure, similar to the one in the first image, is shown in a dark field. The structure is roughly circular with a bright, glowing center. The outer boundary is slightly irregular and appears to have some internal structure or texture. The background is dark with some faint, scattered light spots.	
25		 A circular structure, similar to the ones in the previous images, is shown in a dark field. The structure is roughly circular with a bright, glowing center. The outer boundary is slightly irregular and appears to have some internal structure or texture. The background is dark with some faint, scattered light spots.	

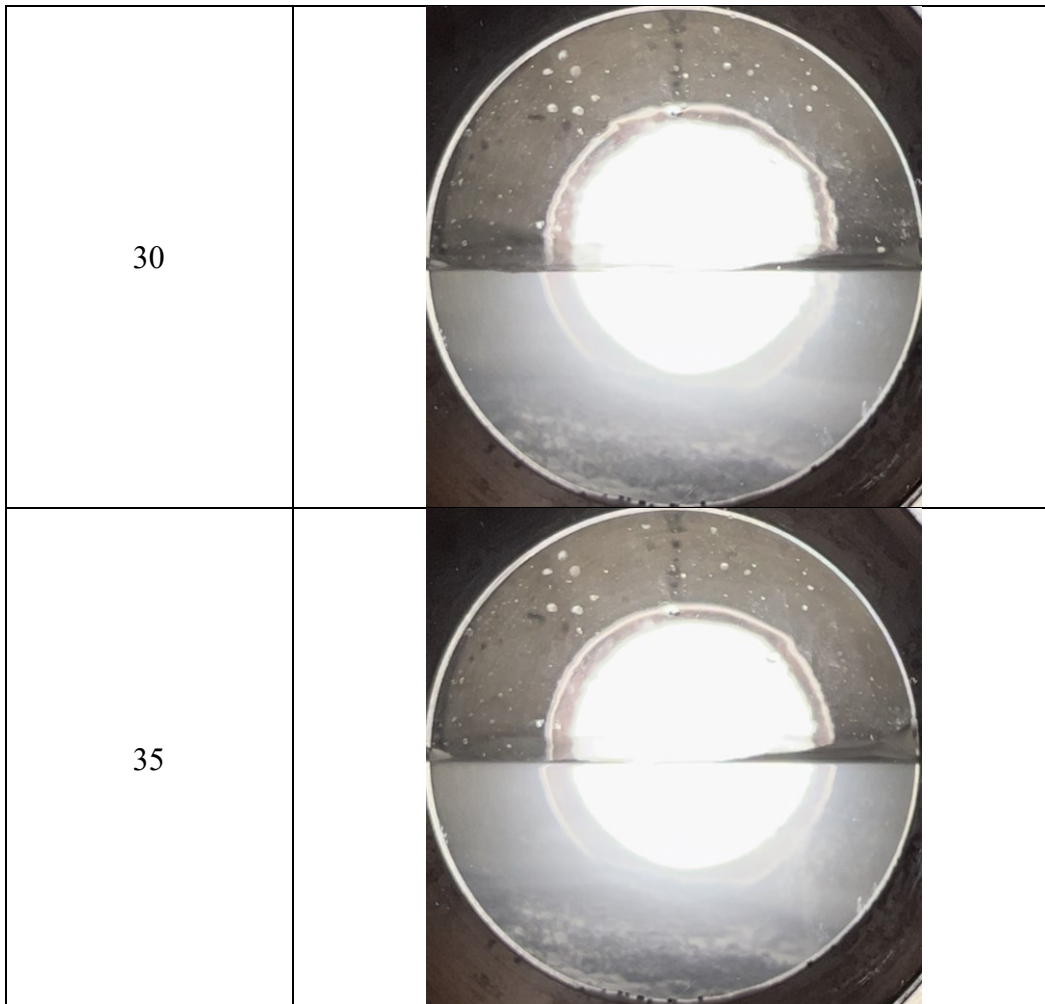


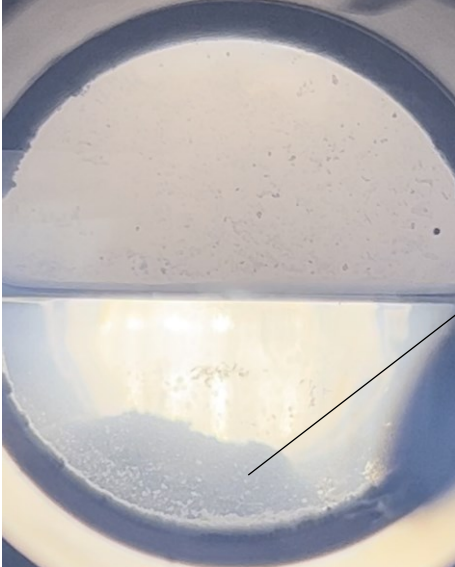
Figure 3.5 Images captured during the process of acid injection into the reactor

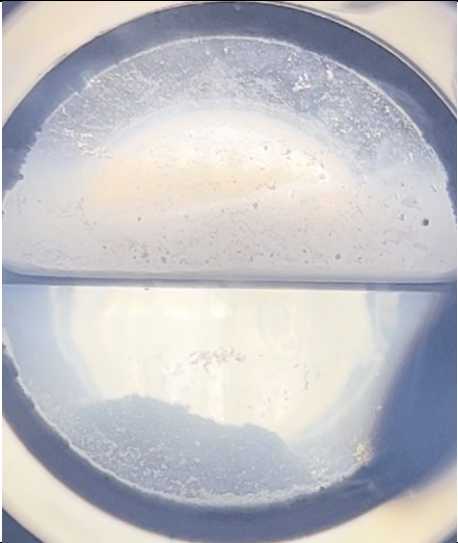
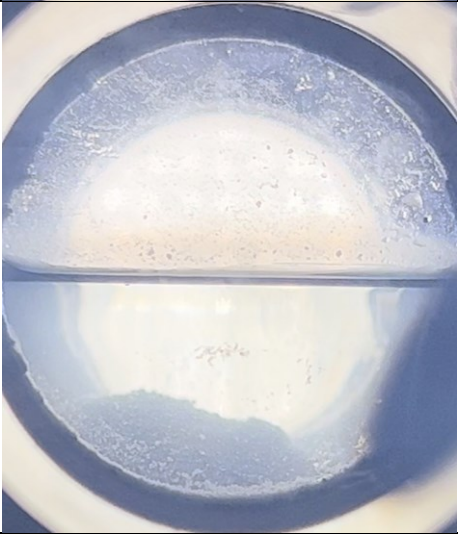
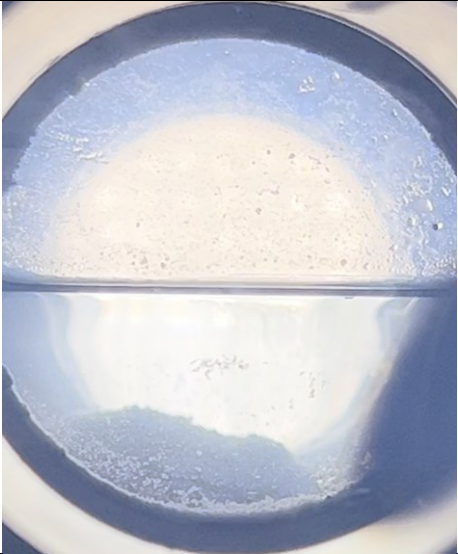
Figure 3.5 shows the images captured during the injection of acetic acid into the reactor. The acid injection causes the liquid level to rise. The reaction seems unspontaneous as the acid and base are under a high-pressure environment. This phenomenon follows the Le Chatelier's principle (Anderson, 2022), i.e., the equilibrium of chemical reactions is shifted due to the changes in the environment, such as pressure, temperature, and concentration. In this case, the equilibrium of the acid-base reaction is shifted to the left, which is unfavourable to produce CO_2 due to the high-pressure environment. In another dry run test,

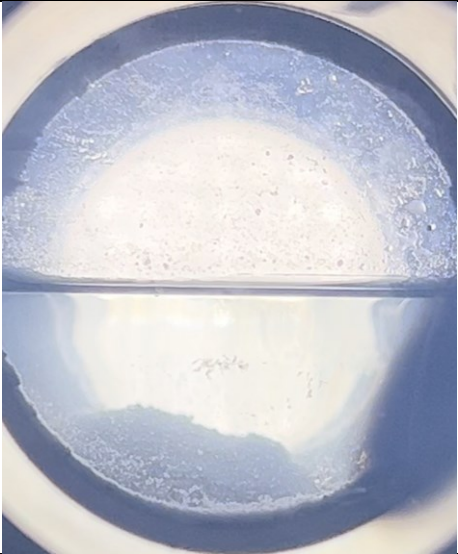
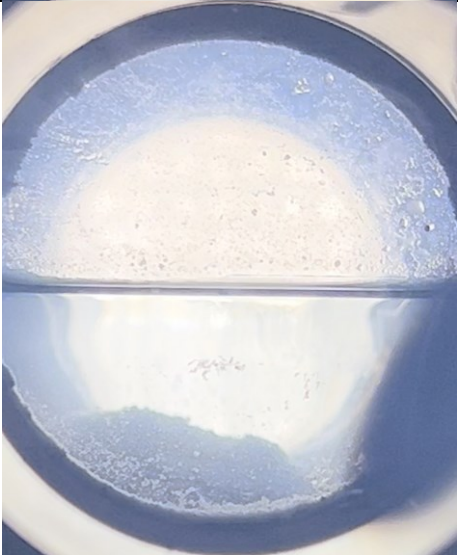
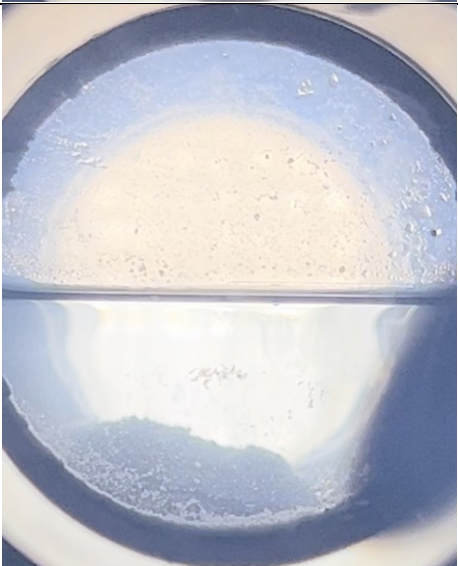
we try to increase the concentration of the reactants to compensate for the effect of pressure, but it does not work.

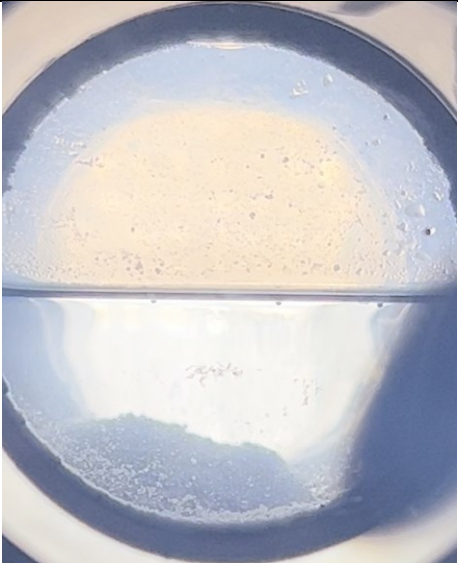
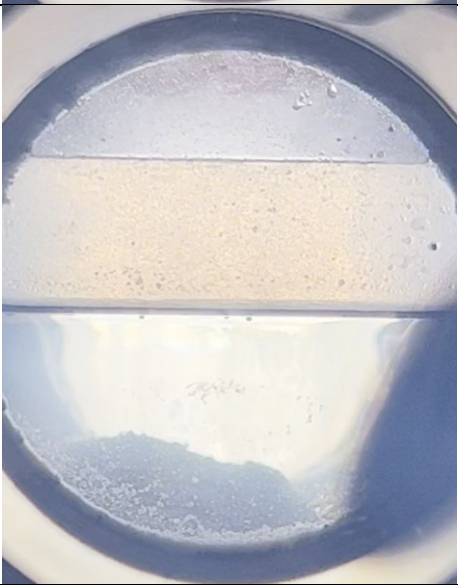
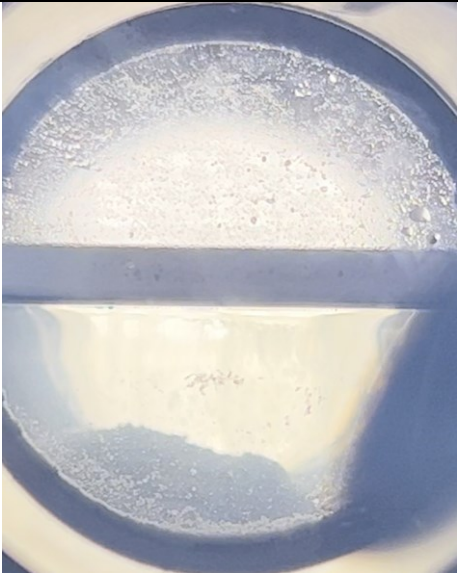
3.3.3 Effect of pressure decline rates

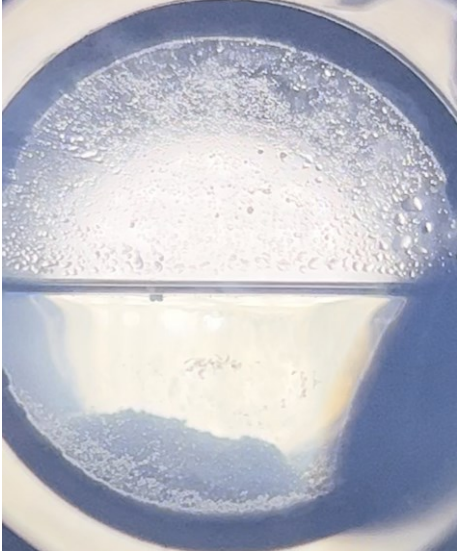
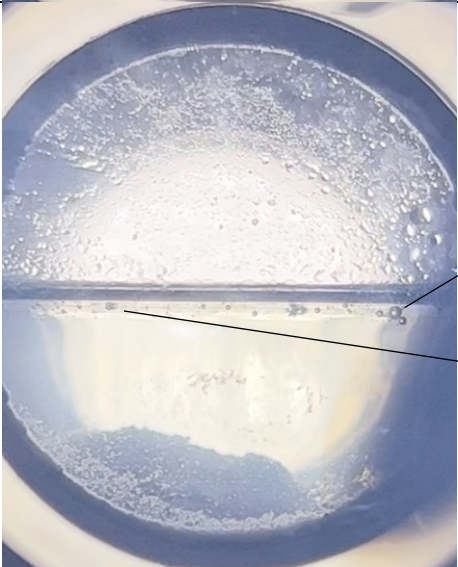

After the pressure in the reactor reaches 14.5 MPa, the acid injection stops. We manage to bleed the pressure in the reactor to 10 MPa. During this process, there are no visible changes in the reactor. We wait 10 minutes for the reading on the pressure to stabilize. After the pressure in the reactor reaches 10 MPa, we adopt two distinctive pressure decline rates to analyze the effect of pressure decline rates on proppant placement efficiency. Figures 3.6 and 3.7 illustrate the proppants distribution states under two pressure decline rates (0.69 MPa/min and 5 MPa/min).

Time, min	The images of the inner reactor during the process of pressure decline (rate: 0.69 MPa/min)
1	 <p data-bbox="1252 1203 1601 1304">Proppant bed + sodium bicarbonate</p>

2			
3			
4			

5			
6			
7			

8			
9			
10			

11			
12			<p data-bbox="1252 867 1601 961">CO₂ bubbles are first observed at 12th minute</p> <p data-bbox="1287 1066 1609 1161">Small number of proppants are floating</p>
13			

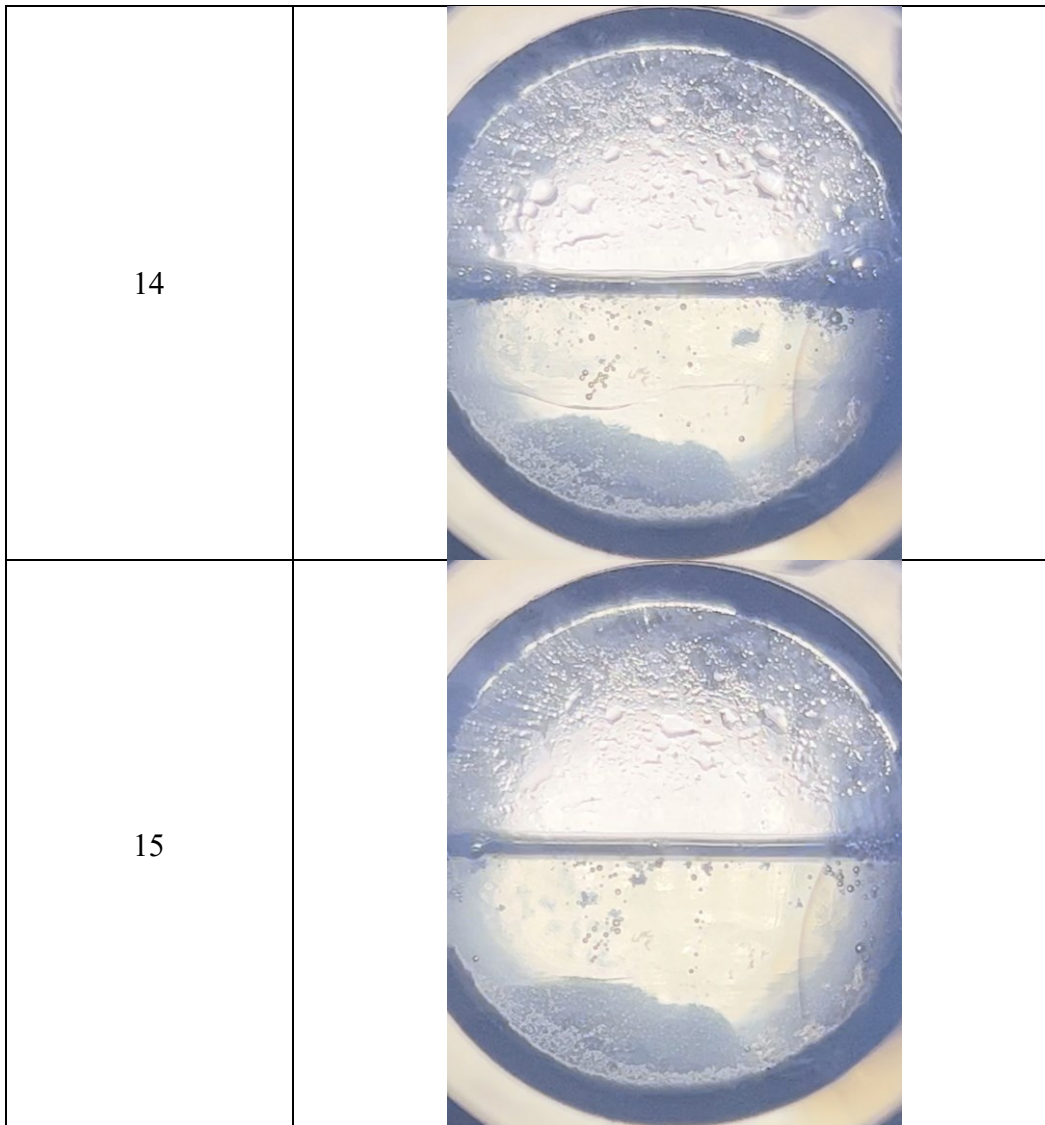
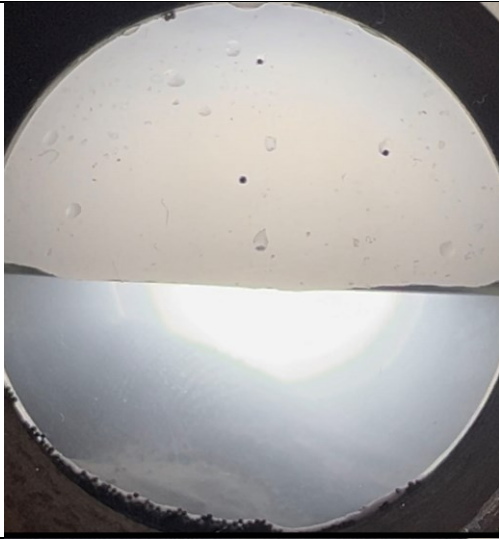





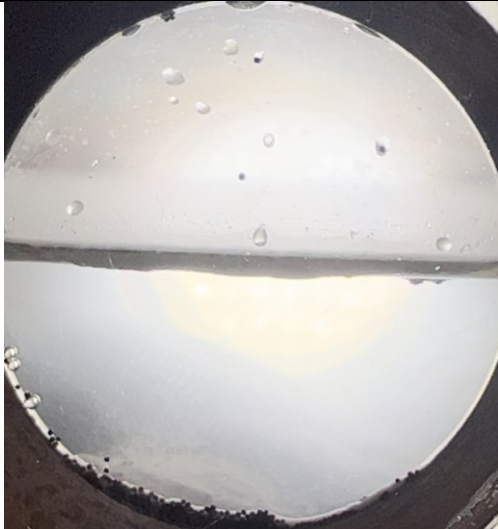

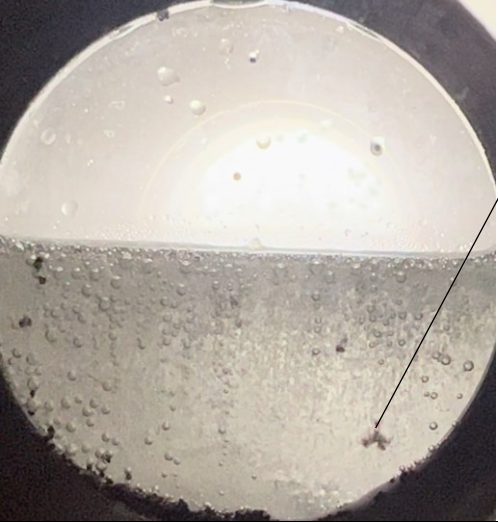


Figure 3.6 Proppant distribution states in the reactor at different times at a pressure decline rate of 0.69 MPa/min

Time, s	The images of the inner reactor during the process of pressure decline (rate: 5 MPa/min)	
10		
20		
30		

40			
50			
60			

70			
80			<p>Small CO₂ bubbles are starting to generate intensively</p>
90			<p>Proppant aggregates are being lifted up.</p>

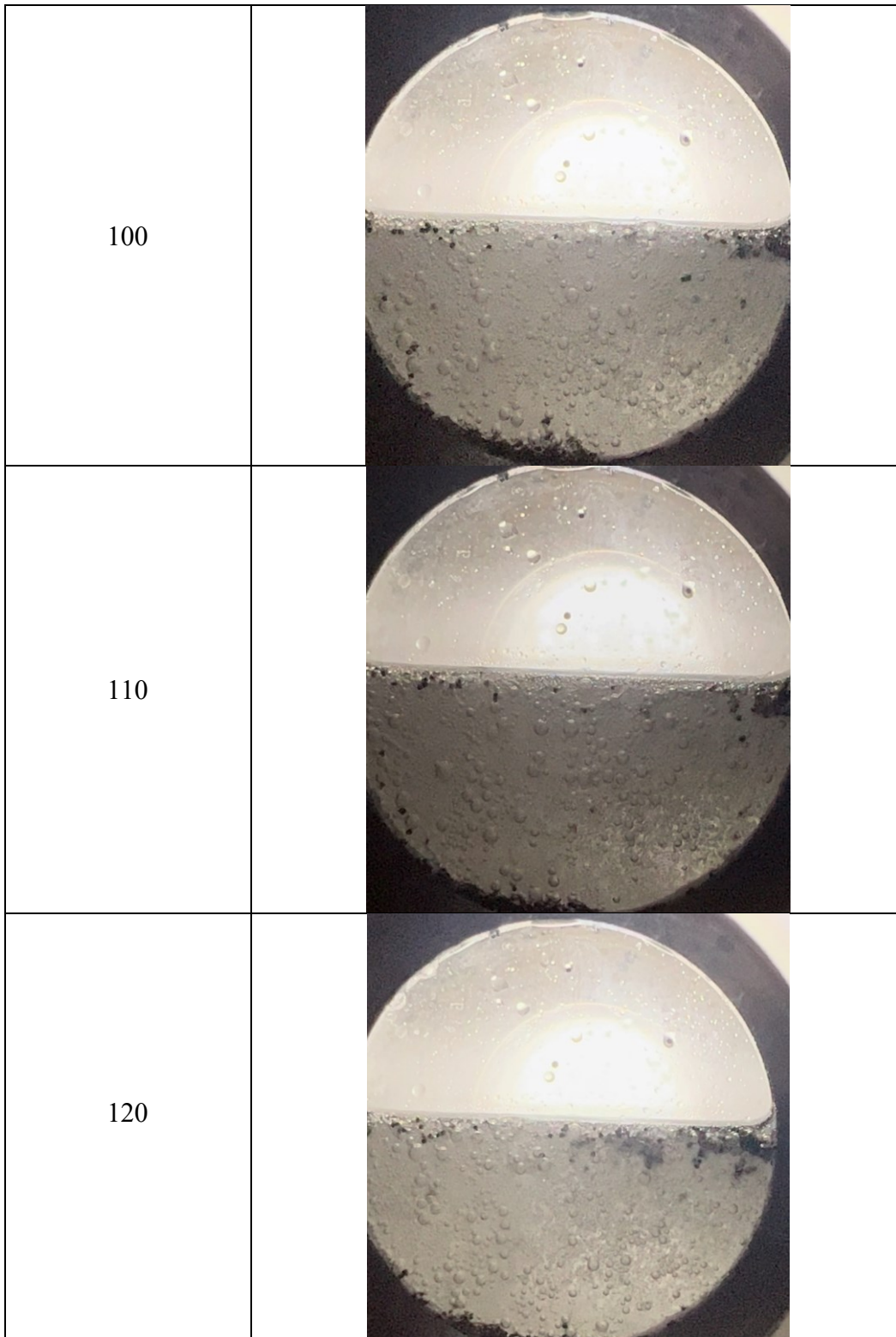


Figure 3.7 Proppant distribution states in the reactor at different times at a pressure decline rate of 5 MPa/min

Based on the results shown in Figures 3.6 and 3.7, we can conclude that a high pressure decline rate of 5 MPa/min can increase the proppant placement efficiency significantly. Under the low pressure decline rate as shown in Figure 3.6, the CO₂ bubbles come out from the solution slowly, and the acid-base reaction is less vigorous compared to the acid-base reaction under the high pressure decline rate. At around 12th min, the reaction-generated CO₂ bubbles are observed, and proppants start to be agitated by CO₂ bubbles. Proppants attach to the gas bubbles and move up and down, but their motions are restricted inside the fracturing fluid, and only around 10% of proppants in the proppant bed are agitated by CO₂ bubbles. Even after the experiment, over 90% of resin-coated proppants remain stationary on the proppant bed. Consequently, the proppant placement efficiency under the low pressure decline rate is extremely low. In comparison, the proppant placement efficiency has increased significantly under the high pressure decline rate condition. As shown in Figure 3.7, the spontaneous acid-base reaction leads to a high CO₂ generation rate due to the fast relief of pressure in the reactor. The reaction-generated gas bubbles, together with the released solution-gas bubbles, work together to push proppants upward. Chemical and mechanical force are both present in this process. Upon the completion of the experiment under the high pressure decline rate, the distribution of proppants inside the reactor is more uniform than the distribution of proppants under the low pressure decline rate. Moreover, the pressure decline rate we apply in this experiment is less than half of the pressure decline rate on the field. Thus, we predict that applying the self-generated gas floating technique in the field may yield a better proppant placement efficiency. However, it is observed that gas bubbles are first generated and start to lift proppants 80 seconds after the experiment starts; at this moment, the corresponding

pressure in the reactor is around 2.5 MPa. This implies that the self-generated gas floating technique may be limited to shallower wells with lower hydrostatic pressures since the reactions seems to be only spontaneous under low pressures. Thus, the feasibility of the self-generated gas floating technique in deeper wells requires further investigation.

3.4 Conclusions

To demonstrate the applicability of the self-generated gas floating technique, we simulate the application of this technique under a high-pressure environment. A reactor with transparent glass windows is used to provide such high-pressure environment. Then, we decrease the pressure in the reactor to simulate the completion stage of a hydraulic fracturing operation. We study the effect of pressure decline rates on proppant placement efficiency by adopting two different pressure decline rates during the tests. We find that the acid-base reaction is unfavourable to occur under a high-pressure environment. This is because the chemical reaction equilibrium shifts when the surrounding environment is unfavourable for reactions (pressure & temperature) (Anderson, 2022). When the pressure decline rate is low, the CO₂ bubbles generate slowly and only agitate a few proppants, leading to a low proppant placement efficiency. When the pressure decline rate is large, a substantial number of CO₂ bubbles are can be generated quickly. Some of the gas bubbles can get attached to the proppants and lift them to the upper part of the reactor.

References

- Anderson, J. G. 2022. University chemistry: frontiers and foundations from a global and molecular perspective. *MIT Press*.
- Bandara, K.M.A.S., Ranjith, P.G., Rathnaweera, T.D., Wanniarachchi, W. A. M., Yang, S. 2021. Crushing and embedment of proppant packs under cyclic loading: an insight to enhanced unconventional oil/gas recovery. *Geoscience Frontiers*, 12(6): 100970.
- Belyadi, H., Fathi, E., Belyadi, F. 2019. Hydraulic fracturing in unconventional reservoirs. *Gulf Professional Publishing*.
- Detournay, Emmanuel., Carbonell, Roberto. 1997. Fracture-mechanics analysis of the breakdown process in minifracture or leak-off test. *SPE Production and Facilities*, 12(3): 195-199
- Khan, J. A., Padmanabhan, E., Haq, I. U. 2020. Hydraulic fracture conductivity in shale reservoirs, in “Emerging technologies in hydraulic fracturing and gas flow modelling”. *IntechOpen*.
- Mehmood, F., Hou, M. Z., Liao, J., Haris, M., Cao, C., Luo, J. 2021. Multiphase multicomponent numerical modeling for hydraulic fracturing with n-heptane for efficient stimulation in a tight gas reservoir of Germany. *Energies*, 14(11): 3111.
- Saunders, P. 2019. Hydraulic fracturing and public health. Encyclopedia of environmental health (second edition). *Elsevier*.
- Shojaei, A., Shao, J. 2017. Porous rock fracture mechanics. *Woodhead Publishing*.
- Wang, F., Ruan, Y., Chen, Q., Zhang, S. 2021. A pressure drop model of post-fracturing shut-in considering the effect of fracturing-fluid imbibition and oil replacement. *Petroleum Exploration and Development*, 48(6): 1440-1449.

Chapter 4: Conclusions and Recommendations

4.1 Conclusions

In this study, the self-generated gas floating technique is introduced to increase the proppant placement efficiency at the upper part of fractures. In Chapter 2, we first prepare extremely hydrophobic proppants by coating a layer of SurfaSil on ceramic proppants. Then, we conduct the contact angle measurements under both atmospheric and aqueous conditions. Finally, we apply the self-generated gas floating technique in a transparent fracture model under ambient conditions and investigate the effect of fracture width, CO₂ generation rate, proppant type, proppant size and gas bubble type on proppant filling efficiency. In Chapter 3, we perform a visual experiment by simulating the application of the self-generated gas floating technique during the completion stage of a hydraulic fracturing operation. We adopt two different pressure decline rates to investigate the effect of pressure decline rate on proppant placement efficiency. The following conclusions can be summarized from this study:

1. By comparing the proppant placement efficiency using ceramic proppants and SurfaSil-treated proppants, we conclude that the higher the degree of hydrophobicity of proppants, the easier it is for proppants to be attached by gas bubbles, leading to a higher proppants placement efficiency.
2. The resin-coated proppants tend to aggregate when being immersed in water, and the aggregation effect is more significant for small proppants. The proppant aggregation effect and strong gas-proppant adhesion force are the reasons why resin-coated proppants usually exhibit the highest proppant placement efficiency.

3. There is a significant adsorption effect of CO₂ on resin-coated proppants. This implies that using CO₂ to attach and lift proppants is advantageous when using resin-coated proppants in fracturing operations.
4. The self-generated gas floating technique will be more effective when using small-size proppants such as proppants with mesh size 30/50. The chemical reaction rate plays an essential role in lifting proppants. It increases the chance of proppants being attached by CO₂ bubbles and provides the kinetic forces to push proppants upward inside fractures.
5. The proppant placement efficiency is lower when the fracture is narrower. The wall effect is significant as it restricts the motion of proppants and gas bubbles. Sometimes, proppant aggregates are stuck in the middle of the fracture and prevent the rise of other proppants.
6. The equilibrium of a chemical reaction can be shifted by surrounding factors. From the high-pressure visual experiments conducted with a see-through reactor, we find that CO₂ cannot be produced through the acid-base reaction under high-pressure conditions. This concurs with the Le Chatelier's principle.
7. A steep pressure decline can initiate the acid-base reaction, releasing the reaction-generated CO₂ bubbles that can lift proppants up inside the reactor. A larger pressure decline rate is more beneficial for applying the self-generated gas floating technique, as we observe a proportional relationship between the proppant placement efficiency and pressure decline rate.

Based on our preliminary stage of investigation, the self-generated gas floating technique may have some limitations when being applied in the field. During the pressure decline

process in the reactor, the gas bubbles first appear when the pressure in the reactor is around 2.5 MPa. The chemical reaction produces more gas bubbles when the pressure is lower than 2.5 MPa. This indicates that the application of self-generated gas floating technique may be limited to shallower wells. In addition, some chemical additives used for preparing the fracturing fluid may not be compatible with sodium bicarbonate or acetic acid. Sodium bicarbonate might react with certain chemical additives, making the chemicals less effective.

4.2 Recommendations

By comparing our experimental conditions with the actual hydraulic-fracturing operation conditions, we find that there are several experimental parameters (such as fracture properties and pressure) that should be tuned to more practically simulate the proppant placement process inside fractures. The fracture model used in our study is made of smooth glass walls with a fixed spacing; the real fractures generated in the field are rough fractures with non-uniform width. In our high-pressure visual experiments, we decrease the pressure in the reactor all the way to zero, which is not the case in the field operations. In field operations, upon the completion of a hydraulic fracturing operation, the fractures are still at least under a high hydrostatic pressure exerted by the fracturing fluids inside the wellbore.

Bibliography

- Abdelbary, A., Li, C. 2023. Principles of Engineering Tribology. *Academic Press*.
- Alghunaim, A., Kirdponpattara, S., Newby, Z. B. M. 2016. Techniques for determining contact angle and wettability of powders. *Powder Technology*, 287: 201-215.
- Anderson, J. G. 2022. University chemistry: frontiers and foundations from a global and molecular perspective. *MIT Press*.
- Bandara, K.M.A.S., Ranjith, P.G., Rathnaweera, T.D., Wanniarachchi, W. A. M., Yang, S. 2021. Crushing and embedment of proppant packs under cyclic loading: An insight to enhanced unconventional oil/gas recovery. *Geoscience Frontiers*, 12(6): 100970.
- Barati, R., Liang, J. T. 2014. A review of fracturing fluid systems used for hydraulic fracturing of oil and gas wells. *Journal of Applied Polymer Science*, 131(16): 40375.
- Belyadi, H., Fathi, E., Belyadi, F. 2019. Hydraulic fracturing in unconventional reservoirs. *Gulf Professional Publishing*.
- Britt, L. K., Smith, M. B., Haddad, Z., Lawrence, P., Chipperfield, S., Hellman, T. 2006. Water-fracs: we do need proppant after all. Paper SPE 102227 presented at the SPE Annual Technical Conference and Exhibition, San Antonio, Texas, USA.
- Buijs, W., Flart, S. 2017. Direct Air Capture of CO₂ with an Amine Resin: A molecular modeling study of the CO₂ capturing process. *Industrial & Engineering Chemistry Research*, 56(43): 12297-12304.
- Cao, W., Xie, K., Lu, X., Chen, Q., Tian, Z., Lin, W. 2020. Self-suspending proppant manufacturing method and its property evaluation. *Journal of Petroleum Science and Engineering*, 192: 107251.

- Danso, D. K., Negash, B. M., Ahmed, T. Y., Yekeen, N., Ganat, T. A. O. 2021. Recent advances in multifunctional proppant technology and increased well output with micro and nano proppants. *Journal of Petroleum Science and Engineering*, 196: 108026.
- Fan, F., Li, F., Tian, S., Sheng, M., Khan, W., Shi, A., Zhou, Y., Xu, Q. 2021. Hydrophobic epoxy resin coated proppants with ultra-high self-suspension ability and enhanced liquid conductivity. *Petroleum Science*, 18(6): 1753-1759.
- Feng, Y. C., Ma, C. Y., Deng, J. G., Li, X. R., Chu, M. M., Hui, C., Luo, Y. Y. 2021. A comprehensive review of ultralow-weight proppant technology. *Petroleum Science*, 18: 807-826.
- Guo, B., Liu, X., Tan, X. 2017. Petroleum production engineering (Second Edition). *Gulf Professional Publishing*.
- Guo, B., Lyons, W. C., Ghalambor, A. 2007. Petroleum production engineering. *Gulf Professional Publishing*.
- Guo, J., Guo, H., Zhang, T., Zeng, X., Li, M., Tang, T. 2022. Experiment on proppant transport in near-well area of hydraulic fractures based on piv/ptv. *Powder Technology*, 410: 117833.
- Guo, S., Wang, B., Li, Y., Hao, H., Zhang, M., Liang, T. 2022. Impacts of proppant flowback on fracture conductivity in different fracturing fluids and flowback conditions. *ACS Omega*, 7(8): 6682-6690.
- Hirpa, M. M., Arnipally, S. K., Bizhani, M., Kuru, E., Gelves, G., Al-Rafia, I. 2020. Effect of particle size and surface properties on the sandbed erosion with water flow in a horizontal pipe. *SPE Journal*, 25(03): 1096-1112.

- Khan, J. A., Padmanabhan, E., Haq, I. U. 2020. Hydraulic fracture conductivity in shale reservoirs, in “Emerging technologies in hydraulic fracturing and gas flow modelling”. *IntechOpen*.
- Li, Y., Zhou, F., Li, B., Cheng, T., Zhang, M., Wang, Q., Yao E., Liang, T. 2022. Optimization of fracturing fluid and retarded acid for stimulating tight naturally fractured bedrock reservoirs. *ACS Omega*, 7(29): 25122-25131.
- Liang, F., Sayed, M., Al-Muntasheri, G. A., Chang, F. F., Li, L. 2016. A comprehensive review on proppant technologies. *Petroleum*, 2(1): 26-39.
- Liang, X., Zhou, F., Liang, T., Huang, Y., Wei, D., Ma, S. 2020. The effect of combined proppants upon the fracture conductivity in tight gas reservoirs. *Energy Reports*, 6: 879-884.
- Liu, P., Huang, Q., Li, J., Du, J., Lu, X., Liu, J., Liu, C., Lan, X. 2023. Review and perspectives of coated proppant technology. *Energy Fuels*, 37(5): 3355-3370.
- Ma, Y. Z., Sobernheim, D., Garzon, J. R. 2015. Unconventional oil and gas resources handbook. *Elsevier*.
- Mack, M. G., Coker, C. E. 2013. Proppant selection for shale reservoirs: optimizing conductivity, proppant transport and cost. Paper SPE 167221 presented at the SPE Unconventional Resources Conference Canada, Calgary, Alberta, Canada.
- Mahoney, R. P., Soane, D. S., Herring, M. K., Kincaid, K. P., Portilla, R. C., Wuthrich, P. 2016. Self-suspending proppants for hydraulic fracturing comprising a coating of hydrogel-forming polymer, USA Patent US9297244B2.

- Mehmood, F., Hou, M. Z., Liao, J., Haris, M., Cao, C., Luo, J. 2021. Multiphase multicomponent numerical modelling for hydraulic fracturing with n-heptane for efficient stimulation in a tight gas reservoir of Germany. *Energies*, 14(11): 3111.
- Montgomery, C. T., Smith, M. B. 2010. Hydraulic fracturing: history of an enduring technology. *Journal of Petroleum Technology*, 62(12): 26-40.
- Rickards, A. R., Brannon, H. D., Wood, W. D., Stephenson, C. J. 2006. High strength, ultralightweight proppant lends new dimensions to hydraulic fracturing applications. *SPE Production & Operations*, 21(02): 212-221.
- Sarmadivaleh, M. 2012. Experimental and numerical study of interaction of a pre-existing natural interface and an induced hydraulic fracture. Doctoral thesis, Curtin University.
- Saunders, P. 2019. Hydraulic fracturing and public health. Encyclopedia of environmental health (second edition). *Elsevier*.
- Shojaei, A., Shao, J. 2017. Porous rock fracture mechanics. *Woodhead Publishing*.
- Soames, A., Al-Ansari, S., Iglauer, S., Barifcani, A., Gubner, R. 2019. Effect of wettability on particle settlement behavior within Mono-Ethylene Glycol regeneration pre-treatment systems. *Journal of Petroleum Science and Engineering*, 179: 831-840.
- Wang, F., Ruan, Y., Chen, Q., Zhang, S. 2021. A pressure drop model of post-fracturing shut-in considering the effect of fracturing-fluid imbibition and oil replacement. *Petroleum Exploration and Development*, 48(6): 1440-1449.



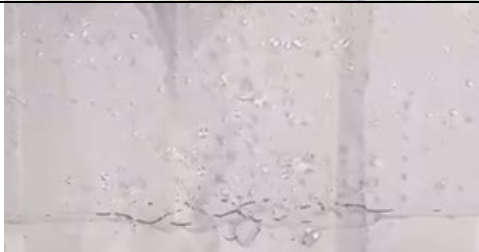
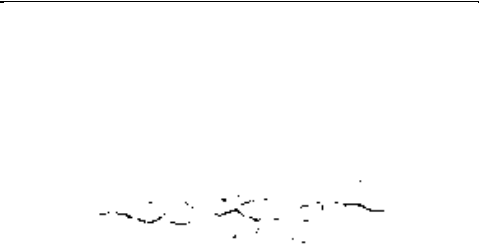

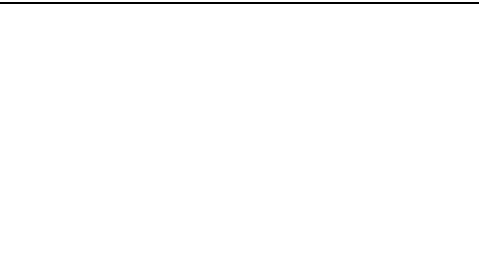
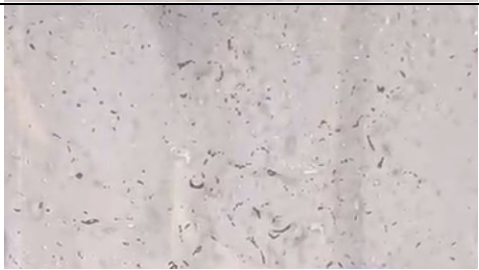
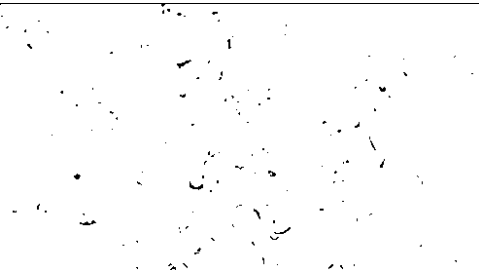

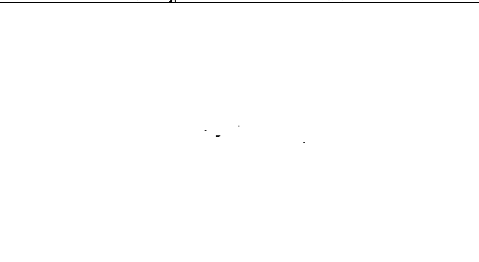
- Wang, J., Elsworth, D. 2018. Role of proppant distribution on the evolution of hydraulic fracture conductivity. *Journal of Petroleum Science and Engineering*, 166: 249-262.
- Wang, L., Li, X., Ding, L., Li, N., Li, X., Liu, X., Zu, K., Meng, L. 2017. The preparation and operational instruction of a gas-suspended proppant for hydraulic fracturing using slick water, China Patent CN106832145A.
- Wang, Q., Chen, X., Jha, A. N., Rogers, H. 2014. Natural gas from shale formation – the evolution, evidences and challenges of shale gas revolution in United States. *Renewable and Sustainable Energy Reviews*, 30: 1-28.
- Wei, G. 2019. Transport Behavior of Resin-Coated Ceramic Proppants in Rough Vertical Fractures. Master thesis, University of Alberta.
- Xiao, D., Wang, M., Guo, B., Weng, D. 2019. Effect of surface wetting behavior of ceramic proppant on the two-phase flow across the interface of sandstone and fracture. *Energy Science & Engineering*, 8(4): 1330-1336.
- Yao, S., Chang, C., Hai, K., Huang, H., Li, H. 2022. A review of experimental studies on the proppant settling in hydraulic fractures. *Journal of Petroleum Science and Engineering*, 208: 109211.
- Yin, Y. B., Yang, Q. S., Wang, S. L., Gao, H. D., He, Y. W., Li, X. L. 2019. formation of co2 bubbles in epoxy resin coatings: a dft study. *Journal of Molecular Graphics and Modelling*, 86: 192-198.
- Zhang, D., Liu, Y., Luo, H., Cao, S., Cao, J., Li, X. 2021. Staged fracturing of horizontal wells in continental tight sandstone oil reservoirs: a case study of yanchang formation in western ordo basin, China. *Frontiers in Earth Science*, 9: 760976.






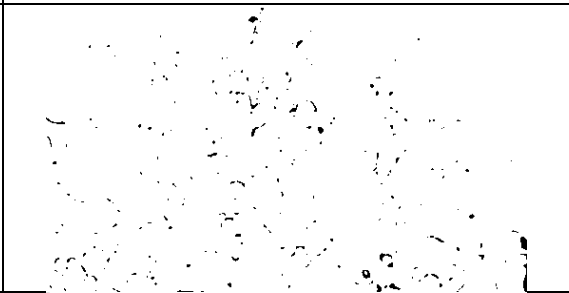






Zhang, J., Liu, K., Cao, M. 2017. Experimental study on modified polyacrylamide coated self-suspending proppant. *Fuel*, 199: 185-190.


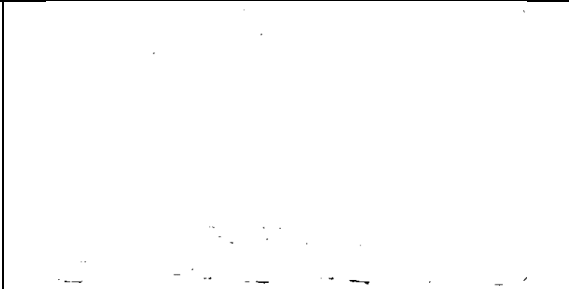
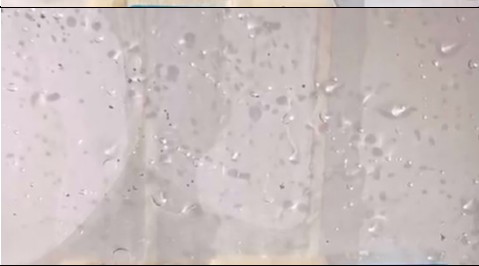
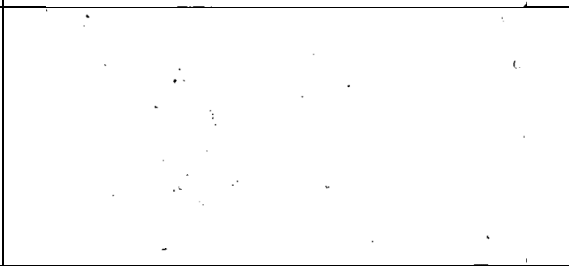





Zhang, Y., Yan, C., Chen, T., Wang, Y. 2016. Ultra-lightweight composite proppants prepared via suspension polymerization. *Journal of Composite Materials*, 50(20):2823-2831.


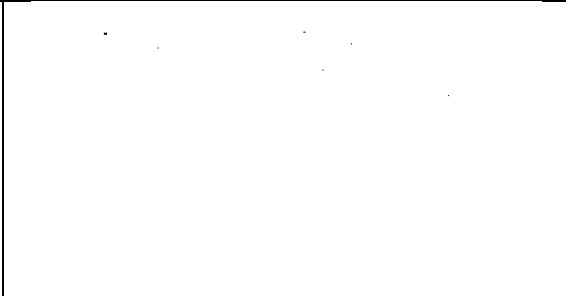






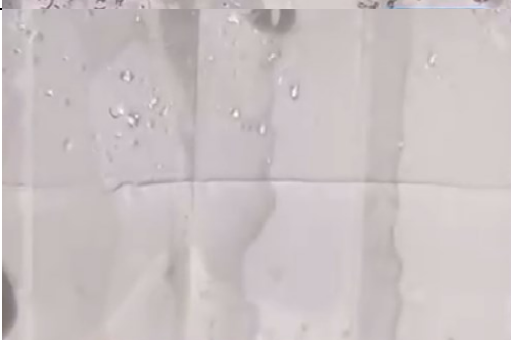
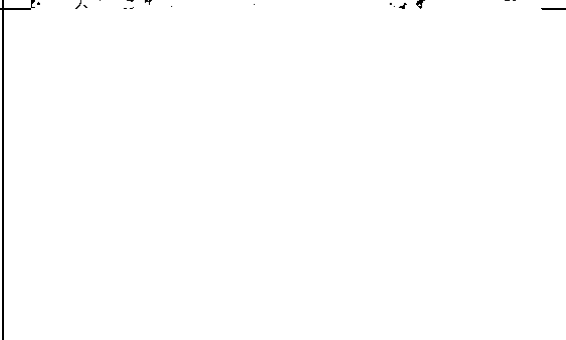
Appendix: Complete Image Analysis Results from the Self-generated Gas Floating Experiments in Chapter 2



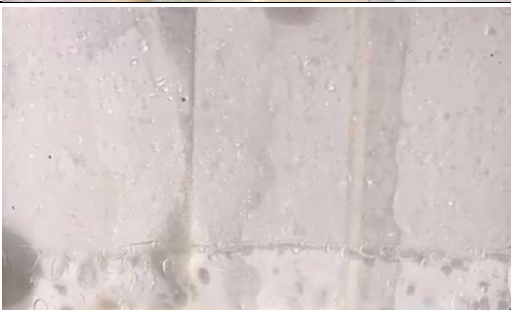


Table A.1 illustrates the results of 60 experiments listed in Table 2.3. The pictures of the fracture model are taken before and after each experiment to accurately demonstrate the increased portion of proppant placement efficiency due to the gas floating effect. The table includes the experimental descriptions, original images, MATLAB processed images and the ratio of the area covered by proppants to the entire area of the fracture model.





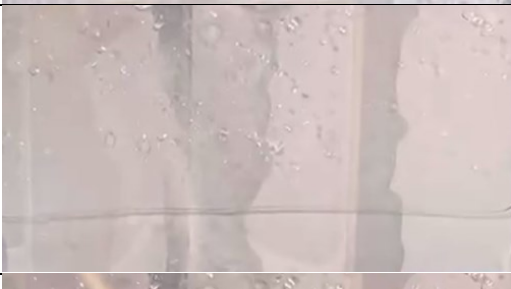

Experimental description (proppant type, proppant size, gas type, fracture width, before or after the experiment)	Original image	Processed image	ratio
RCP, 30/50, air, 1.5mm, before			3.462E-04
RCP, 30/50, air, 1.5 mm, after			3.586E-3
RCP, 30/50, CO ₂ , fast acid injection (21ml/min), low concentration (4 wt% NaHCO ₃), 1.5 mm, before			0
RCP, 30/50, CO ₂ , fast acid injection (21ml/min), low concentration (4 wt% NaHCO ₃), 1.5 mm, after			6.523E-3
RCP, 30/50, CO ₂ , slow acid injection (10ml/min), low concentration (4 wt% NaHCO ₃), 1.5 mm, before			8.869E-5



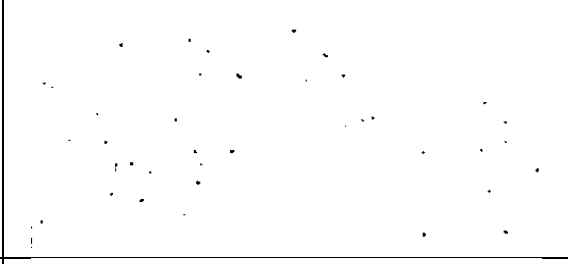




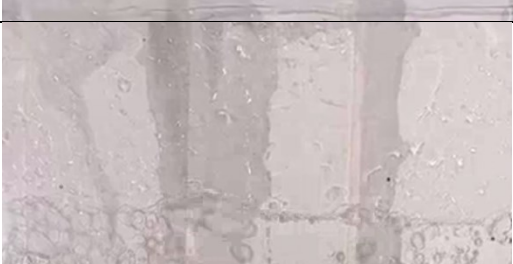
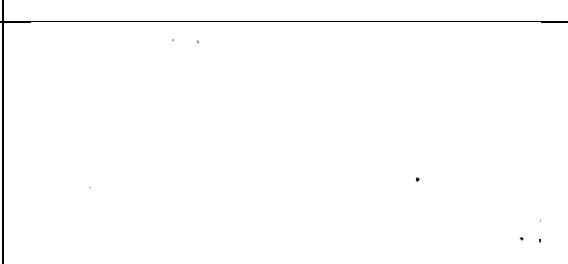
<p>RCP, 30/50, CO₂, slow acid injection (10ml/min), low concentration (4 wt% NaHCO₃), 1.5 mm, after</p>			<p>1.066E-2</p>
<p>RCP, 30/50, CO₂, slow acid injection (10ml/min), high concentration (8 wt% NaHCO₃), 1.5 mm, before</p>			<p>0</p>
<p>RCP, 30/50, CO₂, slow acid injection (10 ml/min), high concentration (8 wt% NaHCO₃), 1.5 mm, after</p>			<p>1.227E-2</p>
<p>RCP, 30/50, CO₂, fast acid injection (21 ml/min), high concentration (8 wt% NaHCO₃), 1.5 mm, before</p>			<p>1.274E-3</p>
<p>RCP, 30/50, CO₂, fast acid injection (21ml/min), high concentration (8 wt% NaHCO₃), 1.5 mm, after</p>			<p>1.116E-2</p>
<p>Treated CP, 30/50, air, 1.5 mm, before</p>			<p>4.927E-4</p>







<p>Treated CP, 30/50, air, 1.5 mm, after</p>			<p>1.023E-3</p>
<p>Treated CP, 30/50, CO₂, fast acid injection (21 ml/min), low concentration (4 wt% NaHCO₃), 1.5 mm, before</p>			<p>7.908E-4</p>
<p>Treated CP, 30/50, CO₂, fast acid injection (21 ml/min), low concentration (4 wt% NaHCO₃), 1.5 mm, after</p>			<p>4.455E-3</p>
<p>Treated CP, 30/50, CO₂, slow acid injection (10 ml/min), low concentration (4 wt% NaHCO₃), 1.5 mm, before</p>			<p>2.734E-4</p>
<p>Treated CP, 30/50, CO₂, slow acid injection (10 ml/min), low concentration (4 wt% NaHCO₃), 1.5 mm, after</p>			<p>3.388E-3</p>







<p>Treated CP, 30/50, CO₂, slow acid injection (10ml/min), high concentration (8 wt% NaHCO₃), 1.5 mm, before</p>			<p>8.792E-5</p>
<p>Treated CP, 30/50, CO₂, slow acid injection (10 ml/min), high concentration (8 wt% NaHCO₃), 1.5 mm, after</p>			<p>8.796E-3</p>
<p>Treated CP, 30/50, CO₂, fast acid injection (21 ml/min), high concentration (8 wt% NaHCO₃), 1.5 mm, before</p>			<p>0</p>
<p>Treated CP, 30/50, CO₂, fast acid injection (21 ml/min), high concentration (8 wt% NaHCO₃), 1.5 mm, after</p>			<p>2.138E-2</p>
<p>CP, 16/30, air, 1.5 mm, before</p>			<p>0</p>






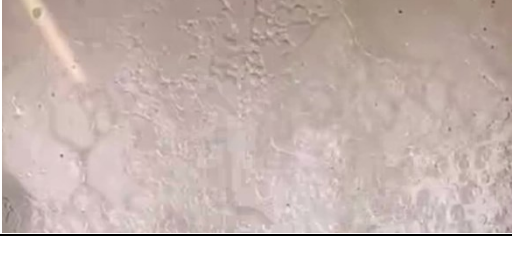
<p>CP, 16/30, air, 1.5 mm, after</p>			<p>1.783E-3</p>
<p>CP, 16/30, CO₂, fast acid injection (21 ml/min), low concentration (4 wt% NaHCO₃), 1.5 mm, before</p>			<p>0</p>
<p>CP, 16/30, CO₂ fast acid injection (21 ml/min), low concentration (4 wt% NaHCO₃), 1.5 mm, after</p>			<p>1.005E-4</p>
<p>CP, 16/30, CO₂, slow acid injection (10 ml/min), low concentration (4 wt% NaHCO₃), 1.5 mm, before</p>			<p>0</p>
<p>CP, 16/30, CO₂, slow acid injection (10 ml/min), low concentration (4 wt% NaHCO₃), 1.5 mm, after</p>			<p>0</p>







<p>CP, 16/30, CO₂, slow acid injection (10 ml/min), high concentration (8 wt% NaHCO₃), 1.5 mm, before</p>			<p>0</p>
<p>CP, 16/30, CO₂, slow acid injection (10 ml/min), high concentration (8 wt% NaHCO₃), 1.5 mm, after</p>			<p>2.931E-5</p>
<p>CP, 16/30, CO₂, fast acid injection (21 ml/min), high concentration (8 wt% NaHCO₃) 1.5 mm, before</p>			<p>0</p>
<p>CP, 16/30, CO₂, fast acid injection (21 ml/min), high concentration (8 wt% NaHCO₃), 1.5 mm, after</p>			<p>0</p>
<p>RCP, 16/30, air, 1.5 mm, before</p>			<p>0</p>
<p>RCP, 16/30, air, 1.5 mm, after</p>			<p>0</p>




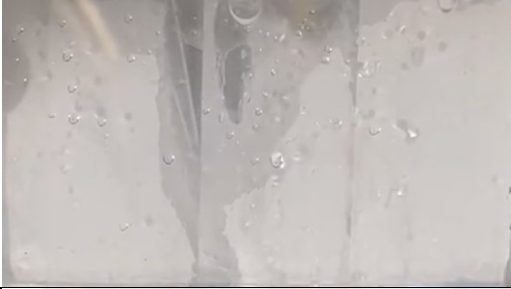


RCP, 16/30, CO ₂ , fast acid injection (21 ml/min), low concentration (4 wt% NaHCO ₃), 1.5 mm, before			0
RCP, 16/30, CO ₂ , fast acid injection (21 ml/min), low concentration (4 wt% NaHCO ₃), 1.5 mm, after			2.117E-3
RCP, 16/30, CO ₂ , slow acid injection (10 ml/min), low concentration (4 wt% NaHCO ₃), 1.5 mm, before			1.114E-4
RCP, 16/30, CO ₂ , slow acid injection (10 ml/min), low concentration (4 wt% NaHCO ₃), 1.5 mm, after			4.793E-4
RCP, 16/30, CO ₂ , slow acid injection (10 ml/min), high concentration (8 wt% NaHCO ₃), 1.5 mm, before			0
RCP, 16/30, CO ₂ , slow acid injection (10 ml/min), high concentration (8 wt% NaHCO ₃), 1.5 mm, after			2.134E-4


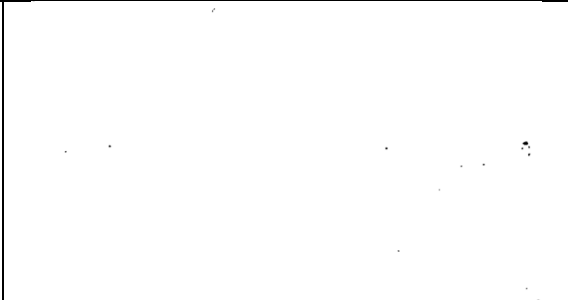



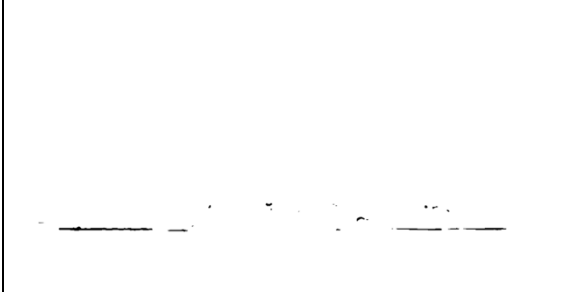




RCP, 16/30, CO ₂ , fast acid injection (21 ml/min), high concentration (8 wt% NaHCO ₃), 1.5 mm, before			0
RCP, 16/30, CO ₂ , fast acid injection (21 ml/min), high concentration (8 wt% NaHCO ₃), 1.5 mm, after			4.800E-5
Treated CP, 16/30, air, 1.5 mm, before			0
Treated CP, 16/30, air 1.5 mm, after			1.934E-4
Treated CP, 16/30, CO ₂ , fast acid injection (21 ml/min), low concentration (4 wt% NaHCO ₃), 1.5 mm, before			0
Treated CP, 16/30, CO ₂ , fast acid injection (21 ml/min), low concentration (4 wt% NaHCO ₃), 1.5 mm, after			3.136E-4









<p>Treated CP, 16/30, CO₂, slow acid injection (10 ml/min), low concentration (4 wt% NaHCO₃), 1.5 mm, before</p>			<p>6.117E-5</p>
<p>Treated CP, 16/30, CO₂, slow acid injection (10 ml/min), low concentration (4 wt% NaHCO₃), 1.5 mm, after</p>			<p>1.240E-4</p>
<p>Treated CP, 16/30, CO₂, slow acid injection (10 ml/min), high concentration (8 wt% NaHCO₃), 1.5 mm, before</p>			<p>0</p>
<p>Treated CP, 16/30, CO₂, slow acid injection (10 ml/min), high concentration (8 wt% NaHCO₃), 1.5 mm, after</p>			<p>3.680E-4</p>
<p>Treated CP, 16/30, CO₂, fast acid injection (21 ml/min), high concentration (8 wt% NaHCO₃), 1.5 mm, before</p>			<p>1.154E-4</p>
<p>Treated CP, 16/30, CO₂, fast acid injection (21 ml/min), high concentration (8 wt% NaHCO₃), 1.5 mm, after</p>			<p>2.171E-4</p>




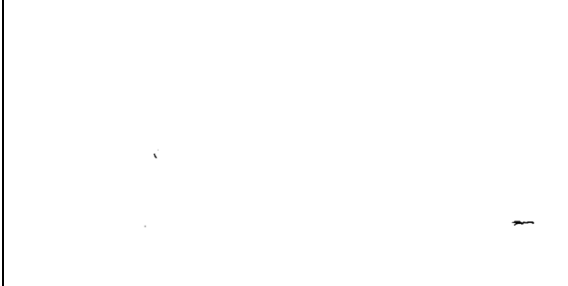

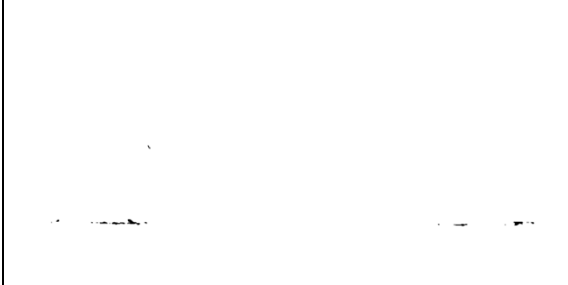

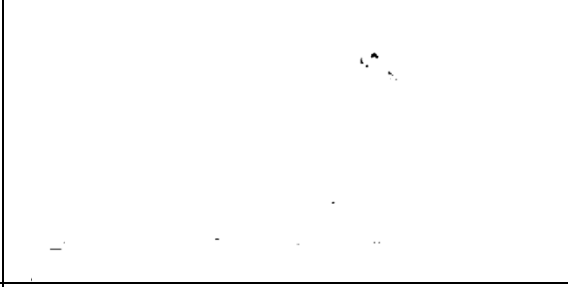

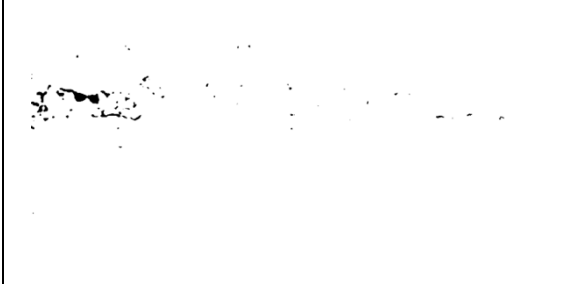
<p>CP, 30/50, air, 1.5 mm, before</p>			<p>0</p>
<p>CP, 30/50, air, 1.5 mm, before</p>			<p>2.391E-4</p>
<p>CP, 30/50, CO₂, fast acid injection (21 ml/min), low concentration (4 wt% NaHCO₃), 1.5 mm, before</p>			<p>1.183E-4</p>
<p>CP, 30/50, CO₂, fast acid injection (21 ml/min), low concentration (4 wt% NaHCO₃), 1.5 mm, after</p>			<p>5.572E-4</p>
<p>CP, 30/50, CO₂, slow acid injection (10 ml/min), low concentration (4 wt% NaHCO₃), 1.5 mm, before</p>			<p>2.261E-4</p>
<p>CP, 30/50, CO₂, slow acid injection (10 ml/min), low concentration (4 wt% NaHCO₃), 1.5 mm, after</p>			<p>4.748E-4</p>







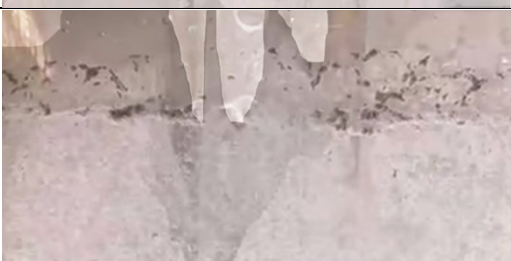
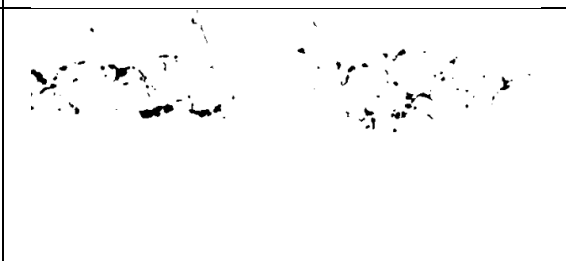

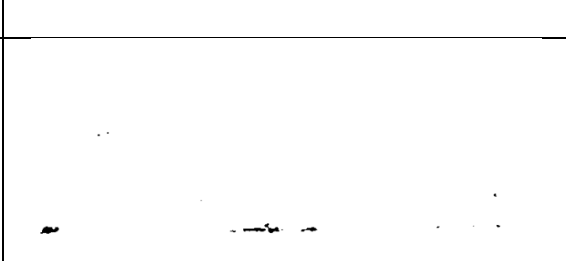

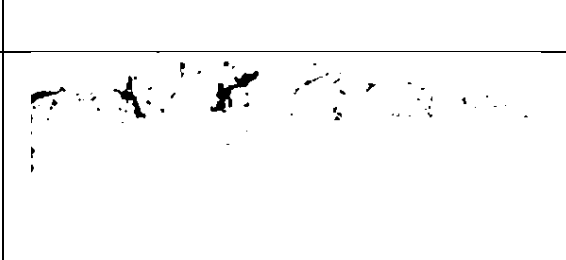
<p>CP, 30/50, CO₂, slow acid injection (10 ml/min), high concentration (8 wt% NaHCO₃), 1.5 mm, before</p>			<p>2.482E-4</p>
<p>CP, 30/50, CO₂, slow acid injection (10 ml/min), high concentration (8 wt% NaHCO₃), 1.5 mm, after</p>			<p>7.328E-4</p>
<p>CP, 30/50, CO₂, fast acid injection (21 ml/min), high concentration (8 wt% NaHCO₃), 1.5 mm, before</p>			<p>9.732E-5</p>
<p>CP, 30/50, air, 1.5 mm, before</p>			<p>2.433E-4</p>
<p>CP, 30/50, air, 4 mm, before</p>			<p>0</p>
<p>CP, 30/50, CO₂, fast acid injection (21 ml/min), low concentration (4 wt% NaHCO₃), 4 mm, before</p>			<p>0</p>







<p>CP, 30/50, CO₂, fast acid injection (21 ml/min), low concentration (4 wt% NaHCO₃), 4 mm, after</p>			<p>4.952E-4</p>
<p>CP, 30/50, CO₂, slow acid injection (10 ml/min), low concentration (4 wt% NaHCO₃), 4 mm, before</p>			<p>0</p>
<p>CP, 30/50, CO₂, slow acid injection (10 ml/min), low concentration (4 wt% NaHCO₃), 4 mm, after</p>			<p>4.368E-4</p>
<p>CP, 30/50, CO₂, slow acid injection (10 ml/min), high concentration (8 wt% NaHCO₃), 4 mm, before</p>			<p>0</p>
<p>CP, 30/50, CO₂, slow acid injection (10 ml/min), high concentration (8 wt% NaHCO₃), 4 mm, after</p>			<p>2.1081E-4</p>
<p>CP, 30/50, CO₂, fast acid injection (21 ml/min), high concentration (8 wt% NaHCO₃), 4 mm, before</p>			<p>4.919E-5</p>







<p>CP, 30/50, CO₂, fast acid injection (21 ml/min), high concentration (8 wt% NaHCO₃), 4 mm, after</p>			<p>2.751E-4</p>
<p>RCP, 30/50, air, 4 mm, before</p>			<p>0</p>
<p>RCP, 30/50, air, 4 mm, after</p>			<p>2.660E-3</p>
<p>RCP, 30/50, CO₂, fast acid injection (21 ml/min), low concentration (4 wt% NaHCO₃), 4 mm, before</p>			<p>0</p>
<p>RCP, 30/50, CO₂, fast acid injection (21 ml/min), low concentration (4 wt% NaHCO₃), 4 mm, after</p>			<p>0.162</p>










<p>RCP, 30/50, CO₂, slow acid injection (10 ml/min), low concentration (4 wt% NaHCO₃), 4 mm, before</p>			<p>0</p>
<p>RCP, 30/50, CO₂, slow acid injection (10 ml/min), low concentration (4 wt% NaHCO₃), 4 mm, after</p>			<p>0.141</p>
<p>RCP, 30/50, CO₂, slow acid injection (10 ml/min), high concentration (8 wt% NaHCO₃), 4 mm, before</p>			<p>9.061E-4</p>
<p>RCP, 30/50, CO₂, slow acid injection (10 ml/min), high concentration (8 wt% NaHCO₃), 4 mm, after</p>			<p>0.323</p>
<p>RCP, 30/50, CO₂, fast acid injection (21 ml/min), high concentration (8 wt% NaHCO₃), 4 mm, before</p>			<p>0</p>







<p>RCP, 30/50, CO₂, fast acid injection (21 ml/min), high concentration (8 wt% NaHCO₃), 4 mm, after</p>			<p>0.283</p>
<p>Treated CP, 30/50, air, 4 mm, before</p>			<p>3.543E-4</p>
<p>Treated CP, 30/50, air, 4 mm, after</p>			<p>7.929E-4</p>
<p>Treated CP, 30/50, CO₂, fast acid injection (21 ml/min), low concentration (4 wt% NaHCO₃), 4 mm, before</p>			<p>3.426E-4</p>
<p>Treated CP, 30/50, CO₂, fast acid injection (21 ml/min), low concentration (4 wt% NaHCO₃), 4 mm, after</p>			<p>4.492E-3</p>

<p>Treated CP, 30/50, CO₂, slow acid injection (10 ml/min), low concentration (4 wt% NaHCO₃), 4 mm, before</p>			<p>8.612E-4</p>
<p>Treated CP, 30/50, CO₂, slow acid injection (10 ml/min), low concentration (4 wt% NaHCO₃), 4 mm, after</p>			<p>1.602E-3</p>
<p>Treated CP, 30/50, CO₂, slow acid injection (10 ml/min), high concentration (8 wt% NaHCO₃), 4 mm, before</p>			<p>6.501E-4</p>
<p>Treated CP, 30/50, CO₂, slow acid injection (10 ml/min), high concentration (8 wt% NaHCO₃), 4 mm, after</p>			<p>0.012</p>
<p>Treated CP, 30/50, CO₂, fast acid injection, (21ml/min) high concentration (8 wt% NaHCO₃), 4 mm, before</p>			<p>1.87E-3</p>
<p>Treated CP, 30/50, CO₂, fast acid injection (21ml/min), high concentration (8 wt% NaHCO₃), 4 mm, after</p>			<p>0.012</p>

<p>CP, 16/30, air, 4 mm, before</p>			<p>0</p>
<p>CP, 16/30, air, 4 mm, after</p>			<p>2.569E-4</p>
<p>CP, 16/30, CO₂, fast acid injection (21 ml/min), low concentration (4 wt% NaHCO₃), 4 mm, before</p>			<p>0</p>
<p>CP, 16/30, CO₂, fast acid injection (21 ml/min), low concentration (4 wt% NaHCO₃), 4 mm, after</p>			<p>3.536</p>
<p>CP, 16/30, CO₂, slow acid injection (10 ml/min), low concentration (4 wt% NaHCO₃), 4 mm, before</p>			<p>0</p>
<p>CP, 16/30, CO₂, slow acid injection (10 ml/min), low concentration (4 wt% NaHCO₃), 4 mm, after</p>			<p>0</p>

<p>CP, 16/30, CO₂, slow acid injection (10 ml/min), high concentration (8 wt% NaHCO₃), 4 mm, before</p>			<p>1.159E-5</p>
<p>CP, 16/30, CO₂, slow acid injection (10 ml/min), high concentration (8 wt% NaHCO₃), 4 mm, after</p>			<p>6.681E-5</p>
<p>CP, 16/30, CO₂, fast acid injection (21 ml/min), high concentration (8 wt% NaHCO₃), 4 mm, before</p>			<p>0</p>
<p>CP, 16/30, CO₂, fast acid injection (21 ml/min), high concentration (8 wt% NaHCO₃), 4 mm, after</p>			<p>0</p>
<p>RCP, 16/30, air, 4 mm, before</p>			<p>0</p>
<p>RCP, 16/30, air, 4 mm, after</p>			<p>9.676E-4</p>

RCP, 16/30, CO ₂ , fast acid injection (21 ml/min), low concentration (4 wt% NaHCO ₃), 4 mm, before			0
RCP, 16/30, CO ₂ , fast acid injection (21 ml/min), low concentration (4 wt% NaHCO ₃), 4 mm, after			1.403E-3
RCP, 16/30, CO ₂ , slow acid injection (10 ml/min), low concentration (4 wt% NaHCO ₃), 4 mm, before			0
RCP, 16/30, CO ₂ , slow acid injection (10 ml/min), low concentration (4 wt% NaHCO ₃), 4 mm, after			1.450E-3
RCP, 16/30, CO ₂ , slow acid injection (10 ml/min), high concentration (8 wt% NaHCO ₃), 4 mm, before			0
RCP, 16/30, CO ₂ , slow acid injection (10ml/min), high concentration (8 wt% NaHCO ₃), 4 mm, after			1.607E-4

<p>RCP, 16/30, CO₂, fast acid injection (21ml/min), high concentration (8 wt% NaHCO₃), 4 mm, before</p>			<p>0</p>
<p>RCP, 16/30, CO₂, fast acid injection (21 ml/min), high concentration (8 wt% NaHCO₃), 4 mm, after</p>			<p>1.528E-4</p>
<p>Treated CP, 16/30, air, 4 mm, before</p>			<p>0</p>
<p>Treated CP, 16/30, air, 4 mm, after</p>			<p>2.455E-4</p>
<p>Treated CP, 16/30, CO₂, fast acid injection (21ml/min), low concentration (4 wt% NaHCO₃), 4 mm, before</p>			<p>5.748E-5</p>
<p>Treated CP, 16/30, CO₂, fast acid injection (21ml/min), low concentration (4 wt% NaHCO₃) 4 mm, after</p>			<p>5.426E-4</p>







<p>Treated CP, 16/30, CO₂, slow acid injection (10ml/min), low concentration (4 wt% NaHCO₃), 4 mm, before</p>			<p>7.813E-5</p>
<p>Treated CP, 16/30, CO₂, slow acid injection (10ml/min), low concentration (4 wt% NaHCO₃), 4 mm, after</p>			<p>3.536E-4</p>
<p>Treated CP, 16/30, CO₂, slow acid injection (10 ml/min), high concentration (8 wt% NaHCO₃), 4 mm, before</p>			<p>1.398E-4</p>
<p>Treated CP, 16/30, CO₂, slow acid injection (10 ml/min), high concentration (8 wt% NaHCO₃), 4 mm, after</p>			<p>9.218E-4</p>
<p>Treated CP, 16/30, CO₂, fast acid injection (21 ml/min), high concentration (8 wt% NaHCO₃), 4 mm, before</p>			<p>1.744E-4</p>
<p>Treated CP, 16/30, CO₂, fast acid injection (21 ml/min), high concentration (8 wt% NaHCO₃), 4 mm, after</p>			<p>1.451E-3</p>

Table A.1 Complete results of the self-generated gas floating experiment in Chapter 2